Real-time Predictive Energy Management of Hybrid Electric Heavy Vehicles by Sequential Programming

N.B. When citing this work, cite the original published paper.

(article starts on next page)

Real-Time Predictive Energy Management of Hybrid Electric Heavy Vehicles by Sequential Programming

Toheed Ghandriz , Bengt Jacobson , Nikolce Murgovski , Peter Nilsson, and Leo Laine

Abstract—With the objective of reducing fuel consumption, this paper presents real-time predictive energy management of hybrid electric heavy vehicles. We propose an optimal control strategy that determines the power split between different vehicle power sources and brakes. Based on model predictive control (MPC) and sequential programming, the optimal trajectories of the vehicle velocity and battery state of charge are found for upcoming horizons with a length of 5–20 km. Then, acceleration and brake pedal positions together with the battery usage are regulated to follow the requested speed and state of charge, which is verified using a high-fidelity vehicle plant model. The main contribution of this paper is the development of a sequential linear program for predictive energy management that is faster and simpler than sequential quadratic programming in tested solvers and provides trajectories that are very close to the best trajectories found by nonlinear programming. The performance of the method is also compared to that of two different sequential quadratic programs.

Index Terms—Predictive energy management strategy, hybrid electric heavy vehicle, optimal control, sequential linear programming.

I. INTRODUCTION

INCREASING concerns about the environment and global warming together with regulations and consumer expectations have motivated the development of new solutions for reducing emissions from road transport. According to [1], heavy-duty vehicles are responsible for 25% of CO_2 emissions from road transport in Europe. Among the different solutions for reducing emissions, energy management control strategies based on road topographic data have been shown to be effective in reducing the fuel consumption of conventional heavy vehicles [2]–[4]. Here, the challenge is to efficiently solve optimal control problems that

can be implemented in real time on board, where the optimal trajectories of the vehicle velocity and gear are found. In [5], an efficient algorithm based on dynamic programming (DP) is presented for optimal control of vehicle speed and gear selection.

Despite the recent improvements in the fuel efficiency of conventional vehicles, emissions from road transport are still rising due to increasing road freight traffic, as reported by [1]. Moreover, according to Regulation (EU) 2018/842, CO_2 emissions of new heavy-duty vehicles shall be reduced by 15% and 30% by the years 2025 and 2030, respectively, compared to those of 2019, forcing the deployment of battery electric and hybrid heavy vehicles to further reduce the emissions caused by road transport and meet the environmental goals.

The problem of energy management of battery electric vehicles is similar to that of conventional vehicles, where the only dynamic state is the vehicle velocity. However, the problem of energy management is more complicated for hybrid electric vehicles (HEVs) since they have multiple power sources. In such vehicles, the regenerative braking energy can be stored and used when the internal combustion engine (ICE) is off or to help the engine function in better operational conditions. HEVs benefit from optimal energy management where the optimal trajectories of the speed, power usage of different power sources and gear selection are found based on the information of the upcoming road. Hence, the size of the optimal control problem of HEVs is larger than that of conventional vehicles, making its efficient solution more challenging.

Different studies have been performed for solving the optimal control problem of HEVs. Model-based solution methods studied in the literature include strategies based on Pontryagin's minimum principle (PMP) and DP. These strategies can also be divided in terms of the dynamic states of the problem and the used simplifications as well as offline and online methods. Methods using PMP are often online and attempt to derive analytic solutions by exploiting the necessary optimality solutions. A well-known example in the HEV energy management field is the equivalent consumption minimization strategy (ECMS) [6], where the battery state of charge in the original problem is replaced with its dual variable. The dynamic original problem is then translated into a two-point boundary-value problem that can be solved efficiently with single shooting techniques. However, the computational advantage of PMP diminishes for problems where the state constraints are frequently activated or integer decisions are required. The problems of frequent active constraints or integer decisions are typically addressed by direct

transcription and then solved numerically. Common examples are the multiple shooting and collocation methods for smooth nonlinear programs [7], [8] or DP and branch, bound and cut techniques for mixed-integer programs [9]–[11] that involve decoupling the speed optimization from power-split and gear optimization or by assuming that the speed profile is known a priori.

DP is also a common method used for energy management of HEVs [12], [13] that requires a high computational effort for the number of states greater than one, which makes it suitable mainly for offline implementations in that case. A comparison between PMP and DP is provided by [6] for a fixed velocity profile.

However, inclusion of speed optimization coupled with battery usage control is important. As discussed in [14], the velocity profile affects the optimal energy management of HEVs. An intuitive example of using the information about the upcoming horizon for optimization of the vehicle velocity is that the velocity can increase on downhill road segments by using only the gravitational force while the engine is off. If the vehicle already has a high velocity prior to reaching a downhill road section, then its capacity for using the gravitational force is reduced because it cannot have a speed higher than the legal maximum speed, and thus, the use of the brakes becomes necessary. The vehicle velocity can be reduced prior to the downhill part of the road, thus avoiding the use of the brakes. In HEVs, the use of regenerative braking is not the best option either because the wheel-to-wheel energy efficiency (i.e., the efficiency of storing the electric energy caused by regenerative braking in the battery and using it for propulsion) is often less than 75%. Therefore, increasing the vehicle velocity using the gravitational force should have priority compared to using electric propulsion. Therefore, considering the velocity as a dynamic state and optimizing its profile have impacts on the energy management of HEVs that are coupled with the power-split and gear optimization. Moreover, inclusion of velocity optimization in energy management helps the vehicle react optimally to traffic disturbances.

For problems comprising two or more continuous states, online control strategies include stochastic DP [15] that predicts future driving cycles and model predictive control where the velocity, state of charge (SOC), and engine on/off and gear profiles are simultaneously optimized, either by combining direct methods, i.e., convex optimization and DP [16], [17], or by combining DP and PMP [18]. Overviews of different methods can be found in [19] and [20].

Solving and validating the actual problem of predictive energy management of HEVs is challenging. In such a problem, the cost function may include components such as fuel and electric energy costs, battery and friction brake wear, and driving comfort. The system state can be described by the vehicle speed, gear ratios, battery energy and engine on/off state, or any other variables related to these characteristics, forming dynamic state variables. In addition, control variables may include ICE power requests, electric machine (EM) power requests on different axles, and gear and braking power requests, depending on the powertrain degrees of freedom. Including all these states and

control variables results in a dynamic, mixed–integer and nonlinear optimal control problem that is very difficult to solve in real time. In this paper, instead, the problem is segregated into three control layers with different horizons and update frequencies, enabling us to test the algorithm using a high-fidelity complex plant vehicle model representing an actual vehicle.

This paper proposes using a sequential linear program (SLP) rather than the sequential quadratic program (SQP) presented in [16], [17], [21] to find optimal trajectories of the vehicle velocity and SOC together with continuous and discrete inputs. The primary benefit of using the SLP is that it is faster than the SQP for the tested solvers, e.g., Gurobi, by a factor of 4 on average for different horizon lengths. The performance of the SLP was compared to that of the SQP in terms of the single sequence computation speed, number of sequential iterations before convergence and obtained optimal trajectories. Moreover, in the SLP, the cost function and constraints were sequentially updated to remove the linearization error. In addition, this paper presents two different SQP methods that are slightly different from the methods previously presented in the literature. In the first SQP, the convex approximation of the fuel rate measurement data was updated during sequential iterations by extracting the positive semidefinite part of the Hessian of the quadratic approximation to ensure convexity. In the second SQP, the quadratic approximating function of the fuel rate was not updated during sequential iterations. However, the included terms of quadratic approximation were selected to keep the approximation always convex for the given measurement data, resulting in a better fit; i.e., the convex approximation was 34% closer to the measurement data compared to similar works [16], [21]–[23] where the quadratic approximation was used for general nonlinear fuel rate measurement data. However, the second SQP does not remove the error caused by the approximation of the fuel rate during sequential iterations. Nevertheless, it requires less computations compared to the first SQP and avoids overfitting the noisy data.

In all three methods, the states are the velocity, battery energy and time, and discrete control variables, namely, gear and engine on/off, are also present. The discrete control variables were handled by solving a secondary optimization subproblem at each sequential iteration in the first control layer. While the gear optimization subproblem is not predictive, it is constrained by the rate of the gearshift. There is no restriction on replacing the instantaneous gear optimization subproblem with a predictive optimal control subproblem, e.g., using DP as presented in [16], [17], [24] with the expense of additional computational effort. Furthermore, in this paper, the engine on/off state was incorporated into the gear selection, where gear number zero indicated an inactive engine and any other number indicated an operating engine.

The rest of the paper is organized as follows. Section II presents a vehicle model together with the nonlinear and mixed–integer optimal control problem. Section III outlines the solution method, including the control hierarchy and sequential linear and quadratic programs. Section IV presents the results. Finally, section V and VI provide a discussion and conclude the paper, respectively.
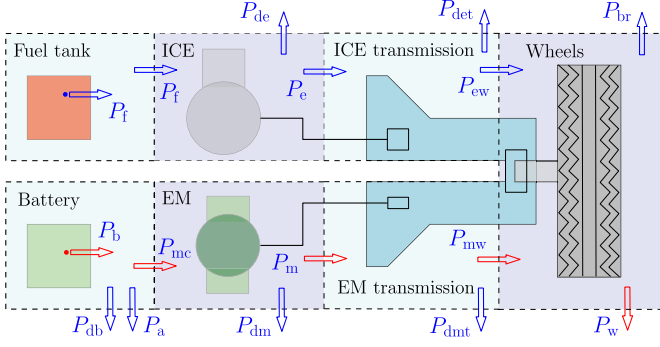
Fig. 1. Energy flow (i.e., input/output power P) in different powertrain subsystems. The arrows illustrate the direction of the energy flow. Red arrows indicate that the energy can also flow in the opposite direction. A dot before an arrow shows a source of power. The subscripts f, e, de, det, ew, br, and w represent fuel, engine, dissipation in engine, dissipation in the transmission from wheels to the engine, engine at wheels, friction brake (or engine brake), and wheels, respectively. Similarly, subscripts b, db, a, mc, m, dm, mw, and dmt represent battery, dissipation in the battery, auxiliaries, motor (i.e., EM) consumption, motor, dissipation in the motor, motor at wheels, and dissipation in the EM transmission, respectively.

II. PROBLEM FORMULATION

A. Vehicle Model

A vehicle is modeled as a lumped mass with wheels that have rolling resistances. The total force at the wheels $F_w(t)$ at time t is given by

$$F_w(t) = m\dot{v}(t) + mg\sin\alpha(s(t)) + mgf_r\cos\alpha(s(t))$$
$$+ 0.5\rho_a A_f c_d v(t)^2, \tag{1}$$

where m is the vehicle total mass or the equivalent total mass, v is the vehicle longitudinal velocity, the three last terms in the right-hand side of Eq. (1) represent the road grade, rolling resistance (modeled as a body force), and air resistance forces, respectively, and g, α, f_r, ρ_a, $s(t)$, A_f and c_d are the gravitational acceleration, road grade, distance traveled at time t, rolling resistance coefficient, air density, equivalent vehicle front area and air drag coefficient, respectively.

Then, the total power $P_w(t)$ needed for the vehicle acceleration and the compensating resistance forces at the wheels is given by

$$P_w(t) = F_w(t)v(t). \tag{2}$$

Fig. 1 illustrates the parallel hybrid powertrain used in this paper and the energy flow (i.e., power) between the different powertrain subsystems. In this figure, at an instance or a given interval of time, for diesel propulsion, P_f, P_e, P_{de}, P_{ew}, and P_{det} denote the fuel power, the power at the ICE output, the power dissipated in the ICE, the power at the ICE transmission output and the power dissipated in the ICE transmission, respectively. On the electric propulsion side, P_b, P_{db}, and P_a denote the power provided by or stored in the battery, dissipated in the battery, and used for the auxiliaries, respectively, and P_{mc}, P_{dm}, P_m, P_{dmt} and P_{mw} denote the power consumed or regenerated by the EM, dissipated in the EM, at the EM output/input to/from the transmission, dissipated in the EM transmission and at the output/input to/from wheels, respectively, and P_{br} is the friction

brake power. No inertial flywheels or elastic shafts are modeled in the powertrain used in this paper. Therefore, for each powertrain subsystem, a power balance can be assumed since no energy is stored or generated inside the powertrain, except in the fuel tank and the battery. For example, the energy balance for the ICE transmission, wheel, and EM transmission can be written as

$$P_{ew} + P_{det} - P_e = 0 \tag{3a}$$

$$P_w + P_{br} - P_{ew} - P_{mw} = 0 \tag{3b}$$

$$P_{mw} + P_{dmt} - P_m = 0, \tag{3c}$$

where the energy flow is positive if energy flows out of a subsystem, e.g. all dissipative terms are positive.

The function arguments are omitted in Eqs. (3) for increased readability. Generally, the powertrain component dissipations are nonlinear functions of the speed, component power, selected ICE gear, γ_e, or EM gear, γ_m. Furthermore, notably, stopping and reversing are not modeled, and the terms describing the inertia of rotating parts in the driveline and wheels and energy loss due to tire slip are neglected. However, the inertia of rotating parts can be considered by using an equivalent additional mass.

Measured data can be used for describing the power dissipation in the ICE and EM for varying torques and angular speeds. The data can be read directly from the maps or be fitted by high-degree nonlinear curves. The torque and angular speed of the ICE and EM are related to their power and the vehicle speed according to

$$\omega_e(t) = \frac{r_e(\gamma_e(t))}{R_w}v(t), \quad T_e(t) = \frac{1}{\omega_e(t)}P_e(t), \tag{4}$$

$$\omega_m(t) = \frac{r_m(\gamma_m(t))}{R_w}v(t), \quad T_m(t) = \frac{1}{\omega_m(t)}P_m(t), \tag{5}$$

where R_w, r_e, T_e, and ω_e are the wheel radius, gear ratio from the wheel to engine, engine torque, and engine speed, respectively, and similarly for the EM, r_m, T_m and ω_m denote the gear ratio from the wheel to EM, EM torque and speed, respectively. Eqs. (4) and (5) are not valid for the neutral gear.

The measurement data can be fitted by a polynomial surface of degree n for the ICE fuel energy rate $\dot{E}_f = P_f$ and EM consumed power P_{mc} as follows; however, any other surface fitting function could also be valid.

$$P_f(\omega_e(t), T_e(t)) = \sum_{i=0}^{n}\sum_{j=0}^{n} a_{ij}\omega_e(t)^i T_e(t)^j, \tag{6}$$

$$P_{mc}(\omega_m(t), T_m(t)) =$$
$$\begin{cases} \sum_{i=0}^{n}\sum_{j=0}^{n} h_{ij}^+\omega_m(t)^i T_m(t)^j, & T_m(t) > 0, \\ \sum_{i=0}^{n}\sum_{j=0}^{n} h_{ij}^-\omega_m(t)^i T_m(t)^j, & T_m(t) \leq 0, \end{cases} \tag{7}$$

where a_{ij}, h_{ij}^+ and h_{ij}^- denote the coefficients of the fitted functions. Fig. 2 shows the measurements and a polynomial surface fitting of degree 5 for the engine fuel energy rate. Using a high degree of the fitted surface resulted in a relatively accurate approximation of the measurement data. Similarly, the fitted surfaces of P_{mc} are illustrated in Fig. 3, where the measurement data
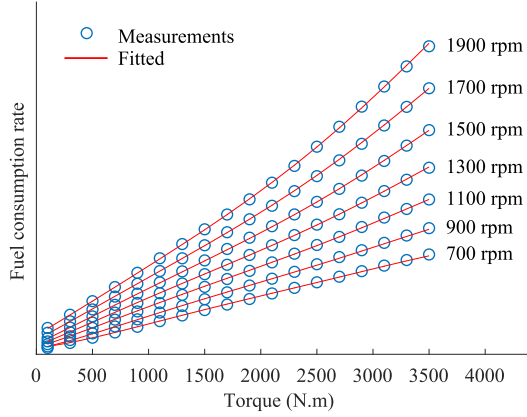
Fig. 2. Fuel consumption rate versus engine torque and speed based on the experimental measurements. The experimental data are fitted by a surface of degree 5.
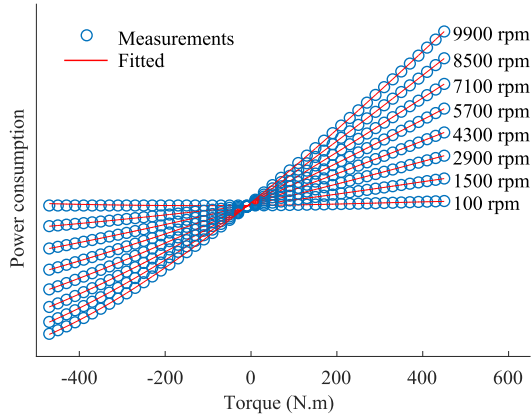

Fig. 3. EM power consumption P_{mc} versus torque and speed based on the experimental measurements. The positive and negative torques are fitted by surfaces of degree 5.

of the positive and negative torques are fitted using two different surfaces to ensure that the EM torque and the EM consumed power P_{mc} have the same sign. The raw measurement data of the power loss in the EM are based on the machine efficiency. The conversion from the efficiency map to the consumed-power map is explained in the Appendix.

The battery can be modeled assuming a constant open-circuit voltage V_b and a resistance R, whereas the voltage drop due to the battery resistance is negligible [23].

$$P_{db}(P_{mc}(t), P_a(t)) = \frac{R}{V_b^2}(P_{mc} + P_a)^2. \quad (8)$$

Furthermore, in this paper, the transmission dissipation is a linear function of the power input independent of the gear selection, and therefore,

$$P_{det}(P_e(t)) = P_e(t) - \eta_{te}P_e(t), \quad P_e(t) \geq 0, \quad (9)$$

and

$$P_{dmt}(P_m(t)) = \begin{cases} P_m(t) - \eta_{tm}P_m(t), & P_m(t) > 0 \\ -(\frac{P_m(t)}{\eta_{tm}} - P_m(t)), & P_m(t) \leq 0, \end{cases} \quad (10)$$

where η_{te} represents the transmission efficiency of the engine and η_{tm} denotes the transmission efficiency of the EM. The dissipation power P_{dmt} is always positive; therefore, a negative sign is necessary in the second part of Eq. (10).

The limits of the powertrain components in transforming energy (or power, force and torque) must also be taken into account. These limits on torques in the engine and EM are shown in Fig. 4 together with piecewise fitted curves. The polynomial fitted curves of degree n for each of the pieces are given by

$$T_{li}(\omega(t)) = \sum_{j=0}^{n} b_{ij}\omega(t)^j, \quad i = 1, \ldots, 4, \quad (11)$$

where T_l denotes the torque limit fitted curve and b_i is the polynomial coefficient.

The capacity and power of the battery are also limited. The battery SOC is given by

$$soc(t_f) = soc(t_0) - \frac{1}{E_{bmax}} \int_{t_0}^{t_f} P_b(t)dt, \quad (12)$$

where E_{bmax} is the battery maximum energy capacity.

B. Nonlinear and Mixed–Integer Problem of Predictive Energy Management

The nonlinear and mixed–integer optimal control problem in this paper is defined as follows.

Find $\quad \boldsymbol{u}_c(s) \in \mathbb{R}^{n_{cc}}, \boldsymbol{u}_d(s) \in \mathbb{N}^{n_{cd}}$

to minimize $\quad J = C(\boldsymbol{x}(s_0), \boldsymbol{x}(s_f))$

$$+ \int_{s_0}^{s_f} L(\boldsymbol{x}(s), \boldsymbol{u}(s), s)ds \quad (13a)$$

subject to $\quad \dfrac{d\boldsymbol{x}(s)}{ds} = \boldsymbol{f}(\boldsymbol{x}(s), \boldsymbol{u}(s), s), \ \boldsymbol{x}(s) \in \mathbb{R}^{n_s} \quad (13b)$

$$\boldsymbol{x}(s_0) = \boldsymbol{x}_0 \quad (13c)$$

$$\boldsymbol{x}(s_f) = \boldsymbol{x}_f \quad (13d)$$

$$\boldsymbol{g}(\boldsymbol{x}(s), \boldsymbol{u}(s), s) \leq 0, \quad (13e)$$

where $\boldsymbol{x}$ represents n_s states, $\boldsymbol{u} = [\boldsymbol{u}_c, \boldsymbol{u}_d]$ represents n_{cc} continuous and n_{cd} discrete control variables, and J, C, s_0, s_f and L represent the cost function, cost of initial and final states, initial position, final position and stage cost function, respectively. Dynamic model equations are given by the constraint equations (13b)-(13d). Finally, constraint equation (13e) restrains the capability of the powertrain components and the bound state and control variables. In the above optimal control problem, any other independent variable instead of position s can be used.

In the case of predictive energy management of HEVs, the road grade profile is described by the position, so it is easier to describe the optimal control problem and the vehicle model with respect to the distance traveled rather than time since this removes the nonlinearity of the road grade as a function of position in the optimal control problem. Moreover, it helps avoid the mixed-integer problem caused by an abrupt change in the road speed limit over distance traveled because modeling the step-change in the speed limit in the time domain yields a
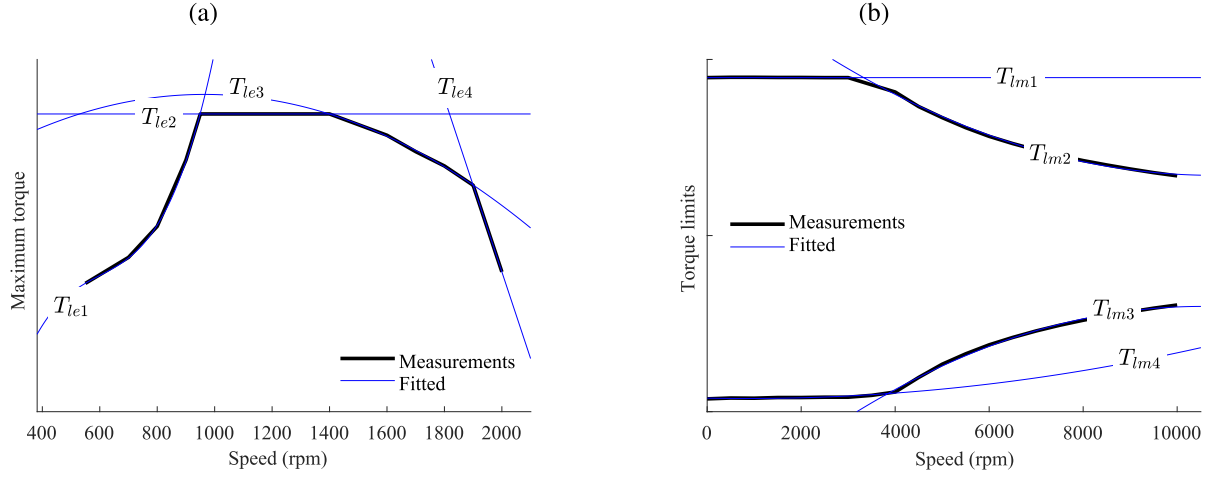
Fig. 4. Torque limit as a function of speed obtained by performing experimental measurements, and the fitted curves: a) Engine, where the fitted curves are T_{le1}-T_{le4}; b) EM, where the fitted curves are T_{lm1}-T_{lm4}.

mixed-integer problem. The conversion from the time to distance s is performed by integrating

$$dt = \frac{ds}{\bar{v}(s)}, \quad \bar{v}(s) = v(t). \tag{14}$$

Basically, $\bar{v}(\cdot)$ and $v(\cdot)$ are different functions; however, $\bar{\ }$ is removed from future equations for simplicity of notation.

Furthermore, the relationships between power P, energy E, force F, torque T and velocity v are given by the following.

$$P(s) = \frac{dE(s)}{dt} = v(s)\frac{dE(s)}{ds} = v(s)F(s) = \omega(s)T(s). \tag{15}$$

The states comprise vehicle velocity v, battery SOC soc, and travel time t, i.e., $\boldsymbol{x} = [v, soc, t]$. The travel time must be introduced as a state since calculation of time is necessary for constraining the total trip time, whereas other equations remain independent of time. Furthermore, the control variables are equivalent engine output force $F_e = \frac{dE_e(s)}{ds}$, EM force on wheels $F_{mw} = \frac{dE_{mw}(s)}{ds}$, brake force on wheels $F_{br} = \frac{dE_{br}(s)}{ds}$, integer gears of ICE γ_e and integer gears of EM γ_m, which are $\boldsymbol{u}_c = [F_e, F_{mw}, F_{br}]$ and $\boldsymbol{u}_d = [\gamma_e, \gamma_m]$. Thereby, using the vehicle model, the nonlinear and mixed–integer optimal control problem of energy management of HEVs can be defined as follows. Notably, the problem below does not have any discrete states. A compact form of the problem in the form of Eqs. (13) where all of the algebraic equations are solved for the state and control variables is given below in this section of the paper.

Find $\quad F_e(s), F_{mw}(s), F_{br}(s), \gamma_e(s), \gamma_m(s)$

to minimize $\quad J^{nl} = \int_{s_0}^{s_f} \left(F_f(\cdot) + F_{br}(s) + F_{del}(s) \right) ds$ (16a)

subject to $\quad F_w(s) = mv(s)\frac{dv(s)}{ds} + mg\sin\alpha(s) +$

$$mgf_r \cos(\alpha(s)) + 0.5\rho_a A_f c_d v(s)^2 \tag{16b}$$

$$\frac{dsoc(s)}{ds} = -\frac{F_b(s)}{E_{bmax}} \tag{16c}$$

$$\frac{dt(s)}{ds} = \frac{1}{v(s)} \tag{16d}$$

$$v(s_0) = v_0, \quad soc(s_0) = soc_0, \quad t(s_0) = t_0 \tag{16e}$$

$$soc(s_f) = soc_f \tag{16f}$$

$$F_w(s) + F_{br}(s) - F_{ew}(s) - F_{mw}(s) = 0 \tag{16g}$$

$$F_{ew}(s) = \eta_{te} F_e(s) \tag{16h}$$

$$F_b(s) = F_{mc}(s) + F_{db}(s) + F_a(s) \tag{16i}$$

$$F_{db}(s) = \frac{Rv(s)}{V_b^2} \left(F_{mc}(s) + F_a(s) \right)^2 \tag{16j}$$

$$F_{mc}(s) = \tag{16k}$$

$$\begin{cases} \frac{1}{v(s)} \sum_{i=0}^5 \sum_{j=0}^5 \left(h_{ij}^+ \left(\frac{r_m(\gamma_m(s))}{R_w} v(s) \right)^i \right. \\ \left. \left(\frac{R_w}{r_m(\gamma_m(s))} F_m(s) \right)^j \right), & F_{mw}(s) > 0 \\ \frac{1}{v(s)} \sum_{i=0}^5 \sum_{j=0}^5 \left(h_{ij}^- \left(\frac{r_m(\gamma_m(s))}{R_w} v(s) \right)^i \right. \\ \left. \left(\frac{R_w}{r_m(\gamma_m(s))} F_m(s) \right)^j \right), & F_{mw}(s) \le 0 \end{cases}$$

$$F_{del}(s) = F_{dmt}(s) + F_{dm}(s) + F_{db}(s) \tag{16l}$$

$$F_{dm}(s) = F_{mc}(s) - F_m(s) \tag{16m}$$

$$F_{dmt}(s) = F_m(s) - F_{mw}(s) \tag{16n}$$

$$F_m(s) = \begin{cases} \frac{F_{mw}(s)}{\eta_{tm}}, & F_{mw}(s) > 0 \\ \eta_{tm} F_{mw}(s), & F_{mw}(s) \le 0 \end{cases} \tag{16o}$$

$$\frac{R_w}{r_e(\gamma_e(s))} F_e(s)$$

$$\leq \min \left\{ \sum_{j=0}^{3} b_{ij}^{e} \left(\frac{r_e(\gamma_e(s))}{R_w} v(s) \right)^{j} , \ i = 1, \ldots, 4 \right\}$$
$$(16\text{p})$$

$$\frac{R_w}{r_m(\gamma_m(s))} F_m(s)$$

$$\leq \min \left\{ \sum_{j=0}^{3} b_{ij}^{m} \left(\frac{r_m(\gamma_m(s))}{R_w} v(s) \right)^{j} , \ i = 1, 2 \right\}$$
$$(16\text{q})$$

$$- \frac{R_w}{r_m(\gamma_m(s))} F_m(s)$$

$$\leq -\max \left\{ \sum_{j=0}^{3} b_{ij}^{m} \left(\frac{r_m(\gamma_m(s))}{R_w} v(s) \right)^{j} , \ i = 3, 4 \right\}$$
$$(16\text{r})$$

$$t(s_f) \leq t_{tref} \tag{16s}$$

$$soc(s) \in [soc_{min}, soc_{max}] \tag{16t}$$

$$v(s)F_b(s) \in [p_{bmin}, p_{bmax}] \tag{16u}$$

$$v_{min}(s) \leq v(s) \leq v_{max}(s) \tag{16v}$$

$$0 \leq F_e(s) \tag{16w}$$

$$0 \leq F_{br}(s). \tag{16x}$$

The cost function J^{nl} in Eq. (16a) is nonlinear, and its minimization represents the minimization of the input engine energy, i.e., fuel E_f, and energy dissipated in the EM E_{del} and by the brakes E_{br}, thereby minimizing their utilization. The energy dissipated in the EM E_{del} was included in the cost function to make later linearization of the EM energy losses possible, as described in later sections. While the brake energy E_{br} does not have to be included in the cost function, it helps achieve faster convergence of the nonlinear program, SQP, and SLP.

The term F_f is the equivalent engine fuel force and can be obtained as follows. Using Eqs. (4) and (6) and surface fitting of degree $n = 5$ together with the change of the variable from time to space, the derivative of the fuel energy consumption with respect to the distance traveled (i.e., the equivalent fuel force) can be derived as

$$F_f(F_e(s), v(s), \gamma_e(s), s)$$
$$= \frac{dE_f(F_e(s), v(s), \gamma_e(s), s)}{ds}$$
$$= \frac{1}{v(s)} \sum_{i=0}^{5} \sum_{j=0}^{5} a_{ij} \left(\frac{r_e(\gamma_e(s))}{R_w} v(s) \right)^{i} \left(\frac{R_w}{r_e(\gamma_e(s))} F_e(s) \right)^{j}.$$
$$(17)$$

Furthermore, Eqs. (16b), (16c) and (16d) are dynamic or state equations equivalent to Eqs. (1), (12) and (14), respectively. Eqs. (16e)-(16f) determine the initial and final values of the states, respectively. Eq. (16g) represents the force equilibrium on the wheels, where F_{ew} represents the equivalent force at the ICE transmission output. Eq. (16h) accounts for energy dissipation

in ICE transmission. Eq. (16i) represents the equivalent force equilibrium in the battery, where F_{mc} represents the equivalent force between the battery and EM given by Eq. (16k), which also accounts for dissipation in the EM for positive and negative torques, similar to Eq. (7), F_{db} is the equivalent force dissipated in the battery given by Eq. (16j), and F_a is the given auxiliary force. Eqs. (16l)-(16o) represent the equivalent dissipated force F_{del} in the electric driveline, which can be derived using Eqs. (3), (15), (7), (8), (10) and (5), where F_{dm} and F_{dmt} represent equivalent forces dissipated in the EM and EM transmission, respectively. Eqs. (16p), (16q) and (16r) impose limits on the torques of the ICE and EM shown in Fig. 4. The total trip time is constrained to be equal to or less than the reference trip time t_{tref} through Eq. (16s), where the method for obtaining the reference trip time is explained in the Appendix. The battery energy level constraint is enforced through limiting battery SOC soc in (16t). Eqs. (16u) and (16v) limit the battery power and vehicle velocity, and finally, Eqs. (16w) and (16x) impose a lower bound on the ICE equivalent force and brake force, respectively.

By solving the algebraic constraints for control variables and performing back-substitution, a compact form of Eqs. (16) is obtained in the form of Eqs. (13).

Find $\qquad F_e(s), F_{mw}(s), F_{br}(s), \gamma_e(s), \gamma_m(s)$

to minimize $\quad J^{nl} = \int_{s=s_0}^{s=s_f} \Big(F_f(\cdot) + F_{br}(s) - F_{mw}(s)$

$$+ F_{mc}(s) + \frac{Rv(s)}{V_b^2} (F_{mc}(s) + F_a(s))^2 \Big) ds$$
$$(18\text{a})$$

subject to $\quad f_1 : \dfrac{dv(s)}{ds} = \dfrac{1}{mv(s)} \big(F_{br}(s) - \eta_{te} F_e(s)$

$$- F_{mw}(s) - mg \sin \alpha(s) - mg f_r \cos \alpha(s)$$
$$-0.5 \rho_a A_f c_d v(s)^2 \big) \tag{18b}$$

$$f_2 : \dfrac{dsoc(s)}{ds} = -\dfrac{1}{E_{bmax}} \Big(F_{mc}(s)$$

$$+ \dfrac{Rv(s)}{V_b^2} (F_{mc}(s) + F_a(s))^2 + F_a(s) \Big)$$
$$(18\text{c})$$

$$f_3 : \dfrac{dt(s)}{ds} = \dfrac{1}{v(s)} \tag{18d}$$

$$v(s_0) = v_0, \quad soc(s_0) = soc_0, \quad t(s_0) = t_0 \tag{18e}$$

$$soc(s_f) = soc_f \tag{18f}$$

$$g_1 : \dfrac{R_w}{r_e(\gamma_e(s))} F_e(s)$$

$$- \min \left\{ \sum_{j=0}^{3} b_{ij}^{e} \left(\frac{r_e(\gamma_e(s))}{R_w} v(s) \right)^{j} , \ i = 1, \ldots, 4 \right\}$$

$$\leq 0 \tag{18g}$$

$$g_3: \quad -\frac{R_{\mathrm{w}}F_{\mathrm{mw}}(s)\eta_{\mathrm{tm}}}{r_{\mathrm{m}}(\gamma_{\mathrm{m}}(s))}$$

$$+ \max\left\{\sum_{j=0}^{3} b_{ij}^{\mathrm{m}}\left(\frac{r_{\mathrm{m}}(\gamma_{\mathrm{m}}(s))}{R_{\mathrm{w}}}v(s)\right)^{j}, \ i=3,4\right\}$$

$$\leq 0 \tag{18h}$$

$$g_4: \quad t(s_{\mathrm{f}}) - t_{\mathrm{tref}} \leq 0 \tag{18i}$$

$$g_5: \quad soc_{\min} - soc(s) \leq 0 \tag{18j}$$

$$g_6: \quad soc(s) - soc_{\max} \leq 0 \tag{18k}$$

$$g_7: \quad p_{\mathrm{bmin}} - v(s)\left(F_{\mathrm{mc}}(s) + \frac{Rv(s)}{V_{\mathrm{b}}^2}(F_{\mathrm{mc}}(s)\right.$$

$$\left. + F_{\mathrm{a}}(s))^2 + F_{\mathrm{a}}(s)\right) \leq 0 \tag{18l}$$

$$g_8: \quad v(s)\left(F_{\mathrm{mc}}(s) + \frac{Rv(s)}{V_{\mathrm{b}}^2}(F_{\mathrm{mc}}(s) + F_{\mathrm{a}}(s))^2\right.$$

$$\left. + F_{\mathrm{a}}(s)\right) - p_{\mathrm{bmax}} \leq 0 \tag{18m}$$

$$g_9: \quad v_{\min}(s) - v(s) \leq 0 \tag{18n}$$

$$g_{10}: \quad v(s) - v_{\max}(s) \leq 0 \tag{18o}$$

$$g_{11}: \quad -F_{\mathrm{e}}(s) \leq 0 \tag{18p}$$

$$g_{12}: \quad -F_{\mathrm{br}}(s) \leq 0, \tag{18q}$$

where $C(\boldsymbol{x}(s_0), \boldsymbol{x}(s_{\mathrm{f}})) = 0$, and F_{mc} is given by Eq. (16k).

A constraint on the acceleration can also be considered . However, it is not directly applied in this paper. The constraints on the acceleration and jerk can be applied in the second control layer in order to increase comfort. However, they are indirectly applied in the first layer through the minimization of the cost function where acceleration and deceleration are discouraged through the use of the propulsion and brake energies.

III. METHOD

A. Control Layers

The overall control hierarchy from the top to bottom layers is depicted in Fig. 5. There are three control layers with different update frequencies. The focus of this paper is the first control layer. However, a short description of other control layers is provided here to give an overview of the vehicle propulsion control system.

The first control layer plans the vehicle velocity v_{req}, energy of the battery soc_{req} and gear trajectories using information from the surrounding environment up to 20 km ahead. The surrounding environment information includes traffic, topography, road curvature, lanes, legal speed limits, dynamic speed limits due to traffic and speed limits due to road curvature; in this paper, road topography and legal speed limit information has been included. The outputs of the first layer are the requested speed, battery SOC and gear trajectories, which are sent to the second and third layers. The gear trajectory includes the neutral state that is equivalent to the ICE being off. In the first layer, the states are
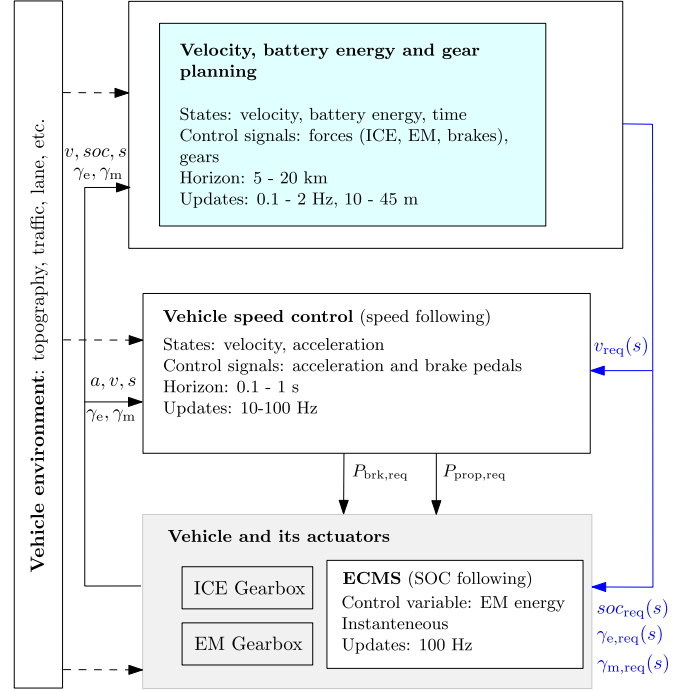

Fig. 5. Overall control hierarchy. The first layer plans vehicle velocity v_{req}, battery SOC soc_{req}, ICE gear $\gamma_{\mathrm{e,req}}$ and EM gear $\gamma_{\mathrm{m,req}}$ for horizons of up to 20 km. The vehicle speed control layer is responsible for tracking the requested speed coming from the first layer by generating the propulsion power $P_{\mathrm{prop,req}}$ and brake power $P_{\mathrm{brk,req}}$ requests, or equivalently the brake and acceleration pedal positions. Finally, the SOC-following control layer that is a part of the vehicle device actuation is responsible for following the SOC trajectory coming from the first layer using the ECMS. Signals a, v, s, soc, γ_{e} and γ_{m} denote feedback signals, i.e., acceleration, velocity, distance traveled, battery SOC, ICE gear and EM gear, respectively.

the velocity, battery energy and time, and the control variables are the ICE, EM, brake force, and gear. Based on MPC theory, optimal trajectories have been found using the SLP or SQP. The gear trajectories serve as inputs to the linear or quadratic programs, while they are sequentially optimized separately in each sequential iteration, converging to a suboptimal trajectory as explained later in this section.

The second and third layers are necessary for compensating the imperfections of the actual road and vehicle that cannot be described by the model used in the first layer. The second layer plans requested propulsion power $P_{\mathrm{prop,req}}$ and brake power $P_{\mathrm{prop,req}}$, or equivalently the brake and acceleration pedal positions. The main objective of this layer is to provide suitable power requests for the vehicle to follow the requested speed trajectory provided in the first layer while guaranteeing comfort and efficiency. This layer was implemented as short horizon MPC similar to the controller presented in [25].

Finally, the third layer is responsible for monitoring and control of device actuation. This layer includes an instantaneous control strategy of battery energy – in particular, the ECMS [6], [26], [27], using the reference SOC trajectory generated in the first control layer.

Notably, when testing the high-fidelity vehicle plant model, it was assumed that the vehicle was equipped with an automatic gearbox that handled gear selection in the best possible manner.
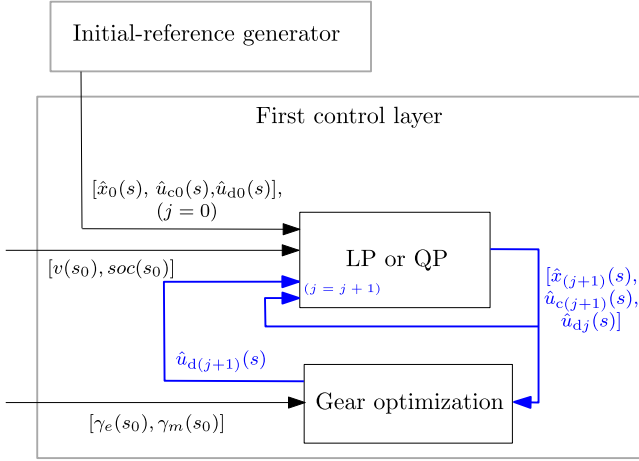
Fig. 6. First control layer and sequential programming. Arrows illustrate data flow, where blue arrows represent data flow in a loop. Upon convergence of the sequential program, $\hat{\gamma}_e(s), \hat{\gamma}_m(s), \hat{v}(s)$ and $s\hat{o}c(s)$ are sent to the next layer as requests, where (ˆ) above a variable indicates that it is a reference value around which linearization is performed. Convergence occurs if the difference between two successive state trajectories is less than a certain value.

Therefore, such a gearbox was allowed to override the gear request coming from the first layer, except for the neutral gear request.

B. Predictive Energy Management Using Sequential Programming

A sequential program solves the optimal control problem sequentially until convergence is reached. First, the problem must be initialized and reference variables, i.e., reference vehicle velocity, engine, and EM energy (or equivalent force) trajectories, must be determined together with the gear trajectory. Then, the sequential program can be performed as follows for a single horizon.

1) Solve the optimal control problem by linear programming (LP) or quadratic convex programming (QP).
2) Update the continuous reference variables, i.e., continuous state and control variables, based on the solution of LP or QP.
3) Solve the gear optimization subproblem to find new reference discrete control variables, i.e., gear trajectory.
4) Stop if convergence is reached; otherwise, go to step 1.

Algorithm 1 and Fig. 6 explain the above stages. In Algorithm 1, (ˆ) above a variable indicates that it is a reference value, i.e., it comes from the previous sequence in sequential programming or is generated by initial–reference generation around which linearization is performed. Initialization of the problem is explained in the Appendix.

LP and QP cannot handle mixed–integer problems. Thereby, this paper finds suboptimal discrete variables, i.e., gears, by solving a heuristic optimization subproblem that is sequentially iterated to reach convergence. The gear optimization subproblem instantaneously finds the best gear $\gamma(s_i)$ by minimizing the energy consumption given the component (i.e., ICE or EM) force and speed; then, starting from position zero, $\gamma(s_{i-1})$ is

---

Algorithm 1: Sequential Programming and Gear Optimization in the First Control Layer.

Input:
Initial states:
$x(s_0) = [v(s_0), soc(s_0), \gamma_e(s_0), \gamma_m(s_0)]$,
initial reference (guess) state trajectories (around which the nonlinear equations will be linearized in the first iteration): $\hat{x}_0(s) = [\hat{v}_0(s), s\hat{o}c_0(s), \hat{t}_0(s)]$,
initial reference (guess) input trajectories:
$\hat{u}_0(s) = [\hat{u}_{c0}(s), \hat{u}_{d0}(s)]$,
where the initial (guess) continuous input trajectories are:
$\hat{u}_{c0}(s) = [\hat{F}_{e0}(s), \hat{F}_{mw0}(s), \hat{F}_{br0}(s)]$
and the initial (guess) discrete input trajectories are:
$\hat{u}_{d0}(s) = [\hat{\gamma}_{e0}(s), \hat{\gamma}_{m0}(s)]$;
Initialization: $j \leftarrow 0$;
1: **while** *not converged***do**
2:     Evaluate the gradient of the cost function and Jacobians of constraints, linearize the constraints, and perform a convex approximation of the cost function if needed to build LP or QP;
3:     Solve the LP or QP by calling the optimization solver to find $x(s)$ and continuous inputs $u_c(s)$;
4:     Solve the two-gear optimization problems (one for the EM and one for the ICE), given $\hat{x}(s)$ and $\hat{u}_c(s)$, to find discrete inputs $u_d(s)$;
5:     Update the state-input guess (reference trajectories) $\hat{x}_j(s)$ and $\hat{u}_j(s) = [\hat{u}_{cj}(s), \hat{u}_{dj}(s)]$ to ensure descent in the Newton direction, e.g., with step size $\alpha \in]0, 1]$ [28]:
$[\hat{x}_{(j+1)}(s), \hat{u}_{c(j+1)}(s)] = [\hat{x}_j(s), \hat{u}_{cj}(s)] + \alpha([x(s), u_c(s)] - [\hat{x}_j(s), \hat{u}_{cj}(s)])$;
$\hat{u}_{d(j+1)}(s) = u_d(s)$
6:     $j \leftarrow j + 1$;
7: **end while**
8: **return** $[\hat{x}_j(s), \hat{u}_{cj}(s), \hat{u}_{dj}(s)]$.

---

updated to $\gamma(s_i)$ if 1) a certain time Δt has passed after the latest gearshift, 2) the fuel conservation is higher than a certain value, and 3) $\gamma(s_{i-1})$ is not feasible anymore. The mentioned three conditions prevent frequent gearshifts.

For the ICE, $\gamma_e(s_i)$ is found as follows for the given position s_i.

Find $\quad\quad \gamma_e(s_i) \in [0, \dots, 12]$

to minimize $\quad F_f(\gamma_e(s)) \quad\quad\quad\quad\quad\quad\quad\quad\quad$ (19a)

subject to $\quad 0 \le \dfrac{R_w}{r_e(\gamma_e(s))}\hat{F}_e(s) \le T_{le}(\dfrac{r_e(\gamma_e(s))}{R_w}\hat{v}(s))$

$\quad\quad\quad\quad\quad\quad\quad\quad\quad\quad\quad\quad\quad\quad\quad\quad$ (19b)

$\quad\quad \omega_{emin} \le \dfrac{r_e(\gamma_e(s))}{R_w}\hat{v}(s) \le \omega_{emax}. \quad\quad$ (19c)

Gearshift is allowed in several steps, e.g., from neutral gear 0 to the highest gear 12 or vice versa. T_{el}, ω_{emin} and ω_{emax} represent engine maximum torque and speed limits according

to Fig. 4. The cost function and constraints of the optimization problem (19) are nonlinear. However, the solution can be found quickly along the horizon due to the low number of feasible gearshifts. A similar optimization problem can be solved for EM gear selection, while in this paper, $\gamma_\mathrm{m}(s) = \hat{\gamma}_\mathrm{m}(s)$ is assumed to be a fixed value. Initial–reference generation is described in Appendix A.

C. Sequential Linear Programming

To derive a linear optimal control problem, the cost function L and constraints f and g should be linearized with respect to the control variables and continuous states $z(s) = [F_\mathrm{e}(s), F_\mathrm{mw}(s), F_\mathrm{br}(s), F_\mathrm{del}(s), v(s), soc(s), t(s)]$ around reference $\hat{z}(s)$, i.e.,

$$L^\mathrm{lin}(z, s) = L(\hat{z}, s) + \nabla^T L(\hat{z}, s)[z - \hat{z}], \tag{20}$$

$$f_i^\mathrm{lin}(z, s) = f_i(\hat{z}, s) + \nabla^T f_i(\hat{z}, s)[z - \hat{z}], i = 1, \ldots, 3, \tag{21}$$

$$g_j^\mathrm{lin}(z, s) = g_j(\hat{z}, s) + \nabla^T g_j(\hat{z}, s)[z - \hat{z}], j = 1, \ldots, 12, \tag{22}$$

where $\nabla = \frac{d}{dz}$ is the gradient operator. The function argument is removed from $z(s)$ for increased readability. Notably, the LP and QP discrete variables are fixed, i.e., $\gamma_\mathrm{e}(s) = \hat{\gamma}_\mathrm{e}(s)$ and $\gamma_\mathrm{m}(s) = \hat{\gamma}_\mathrm{m}(s)$. Obtaining the initial value of these reference trajectories is described in Appendix A. New control variable $F_\mathrm{del}(s)$ has been added as explained below.

Notably, not all of the terms of the cost function and constraints of optimization problem (18) are nonlinear with respect to all state and control variables. Moreover, terms involving F_mc given by Eq. (16k) have two different function descriptions for positive and negative F_mw, which are necessary for accurately modeling electric dissipation. A linear dissipation model can be derived for electric propulsion components. Using Eqs. (16l)-(16n), it can be shown that

$$
\begin{aligned}
F_\mathrm{del}(s) &= F_\mathrm{mc}(s) - F_\mathrm{mw}(s) + F_\mathrm{db}(s) \\
&= F_\mathrm{mc}(s) - F_\mathrm{mw}(s) + \frac{Rv(s)}{V_\mathrm{b}^2}(F_\mathrm{mc}(s) + F_\mathrm{a}(s))^2.
\end{aligned}
\tag{23}
$$

Furthermore, by substituting $F_\mathrm{m}(s)$ from Eq. (16o) into Eq. (16k), it is obtained that

$$
F_\mathrm{mc}(s) =
\begin{cases}
\frac{1}{v(s)} \sum_{i=0}^5 \sum_{j=0}^5 \left(h_{ij}^+ \left(\frac{r_\mathrm{m}(\hat{\gamma}_\mathrm{m}(s))}{R_\mathrm{w}} v(s) \right)^i \right. \\
\left. \left(\frac{R_\mathrm{w} F_\mathrm{mw}(s)}{r_\mathrm{m}(\hat{\gamma}_\mathrm{m}(s)) \eta_\mathrm{tm}} \right)^j \right), \quad F_\mathrm{m}(s) > 0 \\
\frac{1}{v(s)} \sum_{i=0}^5 \sum_{j=0}^5 \left(h_{ij}^- \left(\frac{r_\mathrm{m}(\hat{\gamma}_\mathrm{m}(s))}{R_\mathrm{w}} v(s) \right)^i \right. \\
\left. \left(\frac{R_\mathrm{w} F_\mathrm{mw}(s) \eta_\mathrm{tm}}{r_\mathrm{m}(\hat{\gamma}_\mathrm{m}(s))} \right)^j \right), \quad F_\mathrm{m}(s) \le 0.
\end{cases}
\tag{24}
$$

Therefore, F_del is an explicit nonlinear function of $F_\mathrm{mw}(s)$ and $v(s)$ that can be linearized using first-order Taylor expansion

as follows.

$$
\begin{aligned}
F_\mathrm{del}^\mathrm{lin}(F_\mathrm{mw}(s), v(s), s) &= F_\mathrm{del}(\hat{F}_\mathrm{mw}(s), \hat{v}(s), s) \\
&+ \frac{\partial F_\mathrm{del}(\cdot)}{\partial F_\mathrm{mw}}\Big|_{(\hat{F}_\mathrm{mw}(s), \hat{v}(s))}(F_\mathrm{mw}(s) - \hat{F}_\mathrm{mw}(s)) \\
&+ \frac{\partial F_\mathrm{del}(\cdot)}{\partial v}\Big|_{(\hat{F}_\mathrm{mw}(s), \hat{v}(s))}(v(s) - \hat{v}(s)),
\end{aligned}
\tag{25}
$$

where $\hat{F}_\mathrm{mw}(s)$ and $\hat{v}(s)$ are the reference values determined in the previous SLP sequence.

Eq. (25) is a piecewise linear function of $F_\mathrm{mw}(s)$ with two pieces, for positive and negative values of $F_\mathrm{mw}(s)$. To handle this term in linear programming, the equality constraint was relaxed in this paper, and F_del was introduced as a new control or optimization design variable such that

$$g_{13}: \quad F_\mathrm{del}^\mathrm{lin}(F_\mathrm{mw}(s), v(s), s) - F_\mathrm{del}(s) \le 0. \tag{26}$$

However, the above relaxation enlarges the feasible set by including F_del in the objective function; therefore, we ensured that the optimal solution is tight, i.e., it will not reside in the enlarged feasible region. This means that one of the pieces in Eq. (25) or Eq. (24) holds for equality at the optimal solution. Tightness is intuitively ensured, as the relaxation leads to the generation of higher losses that are minimized by the optimizer. Hence, the optimizer makes the relaxation tight. Further discussion about the tightness of the optimal solution can be found in [29] and [30].

Furthermore, in the cost function, the equivalent engine fuel force F_f given by Eq. (17) is an explicit function of $F_\mathrm{e}(s)$ and $v(s)$ that can be linearized (i.e., affine approximation) using first-order Taylor expansion as

$$
\begin{aligned}
F_\mathrm{f}^\mathrm{lin}(F_\mathrm{e}(s), v(s), s) &= F_\mathrm{f}(\hat{F}_\mathrm{e}(s), \hat{v}(s), s) \\
&+ \frac{\partial F_\mathrm{f}(.)}{\partial F_\mathrm{e}}\Big|_{(\hat{F}_\mathrm{e}(s), \hat{v}(s))}(F_\mathrm{e}(s) - \hat{F}_\mathrm{e}(s)) \\
&+ \frac{\partial F_\mathrm{f}(.)}{\partial v}\Big|_{(\hat{F}_\mathrm{e}(s), \hat{v}(s))}(v(s) - \hat{v}(s)).
\end{aligned}
\tag{27}
$$

Therefore, the linear cost function is obtained as follows.

$$J^\mathrm{lin} = \int_{s_0}^{s_\mathrm{f}} \left(F_\mathrm{f}^\mathrm{lin}(F_\mathrm{e}(s), v(s), s) + F_\mathrm{br}(s) + F_\mathrm{del}(s) \right) ds. \tag{28}$$

Moreover, $F_\mathrm{del}(s)$, which is introduced as a control variable, linearizes constraint f_2 and changes constraints g_7 and g_8 using Eq. (23).

$$f_2: \quad \frac{dsoc(s)}{ds} = -\frac{1}{E_\mathrm{bmax}}(F_\mathrm{mw}(s) + F_\mathrm{del}(s) + F_\mathrm{a}(s)) \tag{29}$$

$$g_7: \quad p_\mathrm{bmin} - v(s)(F_\mathrm{mw}(s) + F_\mathrm{del}(s) + F_\mathrm{a}(s)) \le 0 \tag{30}$$

$$g_8: \quad v(s)(F_\mathrm{mw}(s) + F_\mathrm{del}(s) + F_\mathrm{a}(s)) - p_\mathrm{bmax} \le 0. \tag{31}$$

In addition, more constraints should be defined to determine the linearization trust region. The trust region is a region around the reference in which the approximation remains close to some

extent to the original nonlinear function.

$$g_{14}: \quad \hat{v}(s) - \rho_{\mathrm{v}} - v(s) \leq 0 \tag{32}$$

$$g_{15}: \quad v(s) - \hat{v}(s) - \rho_{\mathrm{v}} \leq 0 \tag{33}$$

$$g_{16}: \quad \hat{F}_{\mathrm{e}}(s) - \rho_1 \hat{F}_{\mathrm{e}}(s) - \rho_0 - F_{\mathrm{e}}(s) \leq 0 \tag{34}$$

$$g_{17}: \quad F_{\mathrm{e}}(s) - \hat{F}_{\mathrm{e}}(s) - \rho_1 \hat{F}_{\mathrm{e}}(s) - \rho_0 \leq 0 \tag{35}$$

$$g_{18}: \quad \hat{F}_{\mathrm{mw}}(s) - \rho_1 \hat{F}_{\mathrm{mw}}(s) - \rho_0 - F_{\mathrm{mw}}(s) \leq 0 \tag{36}$$

$$g_{19}: \quad F_{\mathrm{mw}}(s) - \hat{F}_{\mathrm{mw}}(s) - \rho_1 \hat{F}_{\mathrm{mw}}(s) - \rho_0 \leq 0, \tag{37}$$

where ρ_{v}, ρ_1 and ρ_0 define the boundaries of the trust region that have a direct effect on the convergence rate of the sequential programming. The trust regions for $F_{\mathrm{br}}(s)$, $F_{\mathrm{del}}(s)$, $soc(s)$ and $t(s)$ include their entire feasible range. Constant ρ_0 is used to ensure that $F_{\mathrm{e}}(s)$ and $F_{\mathrm{mw}}(s)$ are not fixed to zero in case of $\hat{F}_{\mathrm{e}}(s)$ and $\hat{F}_{\mathrm{mw}}(s)$ being zero.

D. Sequential Convex Quadratic Programming With an Updating Cost Function

In a convex quadratic program (QP), the cost function is convex quadratic, and the constraints are linear in the state and control variables. Therefore, the only difference between an LP and a QP is that in a QP, cost function (28) should be convex quadratic rather than linear. The only nonlinear term of the cost function is F_{f} given by Eq. (17), which must be approximated by a quadratic function $F_{\mathrm{f}}^{\mathrm{sqp}}$ according to

$$
\begin{aligned}
F_{\mathrm{f}}^{\mathrm{sqp}}(F_{\mathrm{e}}(s), v(s), s) &= F_{\mathrm{f}}(\hat{F}_{\mathrm{e}}(s), \hat{v}(s), s) \\
&+ \frac{\partial F_{\mathrm{f}}(\cdot)}{\partial F_{\mathrm{e}}}\Big|_{(\hat{F}_{\mathrm{e}}(s), \hat{v}(s))}(F_{\mathrm{e}}(s) - \hat{F}_{\mathrm{e}}(s)) \\
&+ \frac{\partial F_{\mathrm{f}}(\cdot)}{\partial v}\Big|_{(\hat{F}_{\mathrm{e}}(s), \hat{v}(s))}(v(s) - \hat{v}(s)) \\
&+ \frac{1}{2}\Bigg[\frac{\partial^2 F_{\mathrm{f}}(\cdot)}{\partial F_{\mathrm{e}}^2}\Big|_{(\hat{F}_{\mathrm{e}}(s), \hat{v}(s))}(F_{\mathrm{e}}(s) - \hat{F}_{\mathrm{e}}(s))^2 \\
&+ 2\frac{\partial^2 F_{\mathrm{f}}(\cdot)}{\partial F_{\mathrm{e}}\partial v}\Big|_{(\hat{F}_{\mathrm{e}}(s), \hat{v}(s))}(F_{\mathrm{e}}(s) - \hat{F}_{\mathrm{e}}(s))(v(s) - \hat{v}(s)) \\
&+ \frac{\partial^2 F_{\mathrm{f}}(\cdot)}{\partial v^2}\Big|_{(\hat{F}_{\mathrm{e}}(s), \hat{v}(s))}(v(s) - \hat{v}(s))^2 \Bigg].
\end{aligned} \tag{38}
$$

However, the quadratic approximation in Eq. (38) is not always convex for all values of s, as the resulting Hessian matrix $H(s)$ is not always symmetric and positive semidefinite. The Hessian matrix can be derived by rearranging the terms of Eq. (38) in the form

$$
\begin{aligned}
F_{\mathrm{f}}^{\mathrm{sqp}}(\cdot) &= [F_{\mathrm{e}}(s), v(s)]^T H(s)[F_{\mathrm{e}}(s), v(s)] \\
&+ f^T(s)[F_{\mathrm{e}}(s), v(s)].
\end{aligned} \tag{39}
$$

In this paper, the convexity of the quadratic approximation has been ensured by extracting the positive semidefinite part of the Hessian matrix so that

$$
\begin{aligned}
F_{\mathrm{f}}^{\mathrm{sqp}}(\cdot) &= [F_{\mathrm{e}}(s), v(s)]^T H^{\mathrm{psd}}(s)[F_{\mathrm{e}}(s), v(s)] \\
&+ f^T(s)[F_{\mathrm{e}}(s), v(s)],
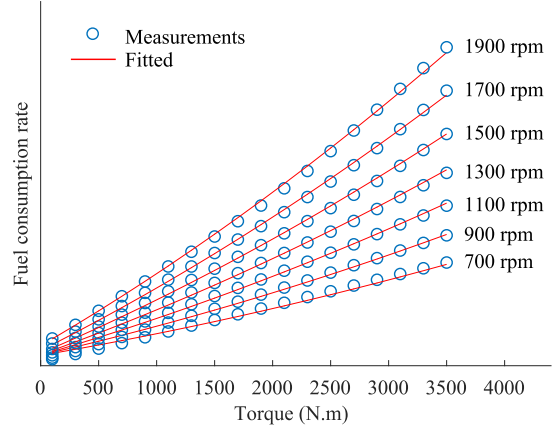\end{aligned} \tag{40}
$$

Fig. 7. Fuel consumption rate versus engine torque and speed obtained by experimental measurements; fitted surface of degree 3 including the following terms: $a_{10}\omega_{\mathrm{e}} + a_{20}\omega_{\mathrm{e}}^2 + a_{11}\omega_{\mathrm{e}}T_{\mathrm{e}} + a_{30}\omega_{\mathrm{e}}^3 + a_{21}\omega_{\mathrm{e}}^2 T_{\mathrm{e}} + a_{12}\omega_{\mathrm{e}}T_{\mathrm{e}}^2$.

where $H^{\mathrm{psd}}(s)$ is the positive semidefinite part of $H(s)$. Hessian matrix $H(s)$ is symmetric. It can be written in the form $Q^T D Q$, where $D = \mathrm{diag}(\lambda_1, \ldots, \lambda_n)$ and λ_i, $i = 1 \ldots n$, are the eigenvalues of the Hessian matrix. Then, matrix D can be written as the sum of two matrices such that $D = D^{\mathrm{pos}} + D^{\mathrm{neg}}$, where D^{pos} and D^{neg} have only positive and negative eigenvalues on the diagonal, respectively. Then,

$$H^{\mathrm{psd}}(s) = Q^T(s)D^{\mathrm{pos}}(s)Q(s). \tag{41}$$

Equation (40) is convex and quadratic in $F_{\mathrm{e}}(s)$ and $v(s)$. Therefore, the quadratic cost function becomes

$$J^{\mathrm{sqp}} = \int_{s_0}^{s_{\mathrm{f}}} (F_{\mathrm{f}}^{\mathrm{sqp}}(F_{\mathrm{e}}(s), v(s), s) + F_{\mathrm{br}}(s) + F_{\mathrm{del}}(s)) \, ds. \tag{42}$$

Notably, matrices $H^{\mathrm{psd}}(s)$ and $f^T(s)$ depend on reference $\hat{F}_{\mathrm{e}}(s)$ and $\hat{v}(s)$ obtained from the previous sequential iteration around which the quadratic approximation is performed. Therefore, the convex quadratic approximation of the cost function is updated in every sequential iteration.

E. Sequential Convex Quadratic Programming With a Non-Updating Cost Function

The calculation of $H^{\mathrm{psd}}(s)$ in Eq. (41) adds to the computational time of the whole SQP, which may not be desirable in real-time application. Alternatively, a surface fitting function of the engine fuel rate can be used as shown in Fig. 7 for improving the convex quadratic approximation of the fuel consumption rate. In this figure, the degree of the polynomial surface fitting is 3, and it is performed to obtain a convex approximation of the engine fuel energy where coefficients a_{00}, a_{01}, a_{02} and a_{03} are zero. By applying the change of variable from time to distance and using the fitted surface, the fuel energy consumption rate P_{f} becomes

$$
\begin{aligned}
P_{\mathrm{f}}(F_{\mathrm{e}}(s), v(s)) &= v(s)F_{\mathrm{f}}(s) \\
&= a_{10}\omega_{\mathrm{e}}(s) + a_{20}\omega_{\mathrm{e}}^2(s) + a_{11}\omega_{\mathrm{e}}(s)T_{\mathrm{e}}(s) \\
&+ a_{30}\omega_{\mathrm{e}}(s)^3 + a_{21}\omega_{\mathrm{e}}(s)^2 T_{\mathrm{e}}(s) + a_{12}\omega_{\mathrm{e}}(s)T_{\mathrm{e}}(s)^2, \tag{43}
\end{aligned}
$$

f_r	0.0047	R (Ω)	0.3
P_{emax} (kW)	552	R_w (m)	0.491
P_{bmax} (kW)	300	η_{te}	0.96
E_{bmax} (kWh)	20	η_{tm}	0.90
V_b (V)	660	r_m	11.9

[0]In addition, $r_e = [39.88, 31.28, 24.11, 18.94, 14.79, 11.59, 9.18, 7.21,$ $5.54, 4.35, 3.40, 2.69]$. The data apply to both 40-ton and 80-ton vehicles. Moreover, $A_f c_d \rho_a = 9.984 \frac{kg}{m}$ for the 80-ton vehicle, and $A_f c_d \rho_a = 4.992 \frac{kg}{m}$ for the 40-ton vehicle. In this paper, the efficiency maps of the ICE and EM are not provided to protect the confidential data.

and after rearranging the terms and using Eq. (4), the quadratic fuel energy consumption can be calculated according to the following.

$$F_f^{qp}(s) = a_{10} \frac{r_e(\hat{\gamma}_e(s))}{R_w} + a_{20} (\frac{r_e(\hat{\gamma}_e(s))}{R_w})^2 v(s) + a_{11} F_e(s)$$

$$+ a_{30} (\frac{r_e(\hat{\gamma}_e(s))}{R_w})^3 v(s)^2 + a_{21} \frac{r_e(\hat{\gamma}_e(s))}{R_w} v(s) F_e(s)$$

$$+ a_{12} \frac{R_w}{r_e(\hat{\gamma}_e(s))} F_e(s)^2. \tag{44}$$

Notably, a quadratic function in the general form given by Eq. (44) is not necessarily convex. However, for the given fuel rate measurement data, Eq. (44) is convex because the resulting Hessian matrix $H(s)$ is always symmetric and positive semidefinite. Moreover, fitting function (43) does not depend on reference $\hat{F}_e(s)$ and $\hat{v}(s)$ and is thus called non-updating even though reference $\hat{\gamma}_e(s)$ updates in every sequential iteration as a solution of the gear optimization subproblem.

IV. RESULTS AND COMPARISONS

A. Comparing the Optimal Solutions Found by SLP, SQP (Updating and Non-Updating) and NLP in the First Control Layer

For solving SLP, SQP and the nonlinear program (NLP), Gurobi LP solver, Gurobi QP solver and MATLAB fmincon function have been used, respectively. Gurobi uses simplex and barrier methods, whereas the interior-point method was used in MATLAB fmincon.

The optimal velocity and SOC trajectories found by applying the three solution methods described above are shown in Fig. 8 for two different vehicle masses of 40 and 80 tons on four different roads, i.e., horizons. The horizon length of approximately 11-13 km is discretized in 300 distance steps using the Euler discretization method, $v_{min} = 5$ m/s, and v_{max} varies based on the road legal speed limit from 18 m/s to 23.6 m/s. The SOCs at the beginning and end of the horizon are constrained to be the same. Several vehicle parameters are shown in Table I . Fig. 8 shows that the optimal trajectories obtained by the SLP are very close to those obtained by the SQP and QP, while the SLP computation time was on average 4 times faster; see Table III. In all cases, the difference in the optimum fuel consumption is less than 1% for different optimization methods; see Table II. An example gear trajectory obtained with the SLP is shown in Fig. 9.

Fig. 10 shows that optimal trajectories obtained by the SLP are very close to those obtained by nonlinear programming.

optimization method	SQP	SQP (non-updating cost)	SLP
max. elevation 49 m	5.961 lit	5.974 lit	5.964 lit
max. elevation 81 m	8.546 lit	8.551 lit	8.544 lit
max. elevation 93 m	8.915 lit	8.941 lit	8.923 lit
max. elevation 113 m	5.541 lit	5.597 lit	5.559 lit

number of stages	60	120	180	240	300	420	580	900
LP (s)	0.01	0.03	0.05	0.08	0.14	0.26	0.63	1.81
QP (s)	0.15	0.17	0.20	0.26	0.31	0.57	1.01	2.71

Nonlinear solutions were obtained using different trajectories of continuous variables as initial guesses for the NLP and with a fixed trajectory of integer variables, i.e., gears, which was obtained by solving the sequential program. The best attained solution is shown in Fig. 10.

The number of iterations or sequences before the SLP and SQP reach convergence is shown in Fig. 11. The SLP and SQP require 3 iterations before the change in the optimal speed reaches well below the speed-following accuracy of the second control layer, i.e., an RMS error of 0.02 m/s versus 0.1 m/s; by contrast, the computational time of the SLP for a sequential iteration is much lower than that of the SQP. Notably, the convergence shown in Fig. 11 refers to sequential convergence of the SLP or SQP. It should not be confused with the internal LP or QP convergence of the optimization solver.

The computation times of the optimization solvers for a single iteration are shown in Table III based on the number of horizon stages, i.e., the road distance steps. The other computations between iterations, including the linearization of the constraints and finding the gears, require 50-100% additional time compared to the time spent by the LP solver for the SLP and SQP with a non-updating cost function. For the SQP with an updating cost function, the between-iteration computations that are needed for the convex approximation of the cost function require 100-200% additional time. Notably, the optimization solver is Gurobi in the MATLAB platform. The use of different solvers on different platforms may reduce the computational time. Moreover, the computational time also depends on the driving cycle and the vehicle powertrain.

Fig. 12 illustrates the optimal trajectories for different horizon lengths. Up to four stages, i.e., approximately 75 m, all the trajectories are alike; this is usually the case for many different horizons with different road profiles. Thus, it can be concluded that the horizon length of approximately 6 km can be sufficient for the given road in this study if the horizon is updated in less than 75 m, corresponding to an available computation time of approximately 3.4 s when driving at the speed of 80 km/h. On the other hand, if the road is flat, the horizon length will not be of much importance. If the horizon is too short, then it may not be able to capture the hill.
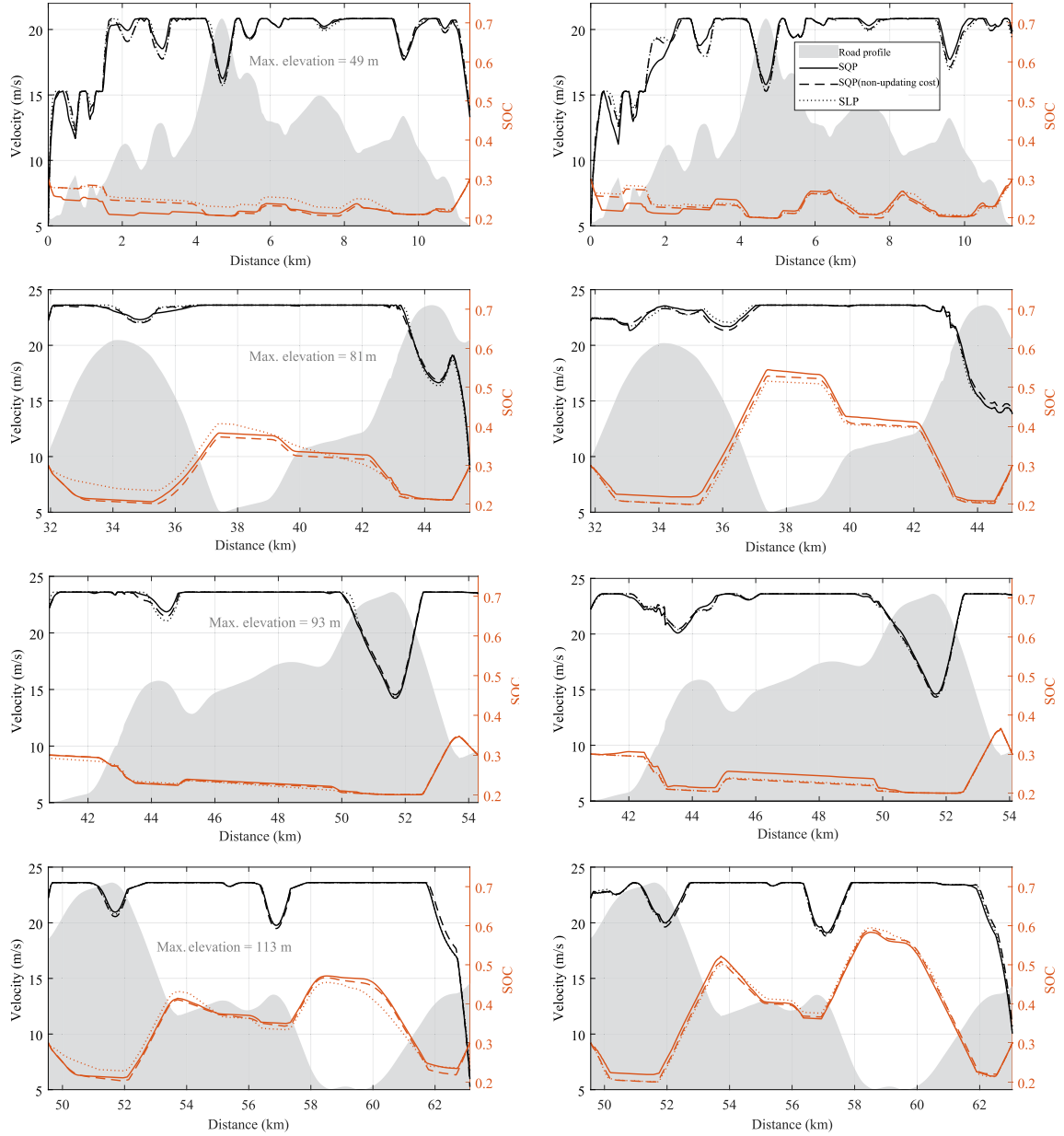
Fig. 8. Comparison of optimal velocities and SOCs obtained by solving the SQP with an updating cost function at each sequential iteration, SQP (with a fixed cost function) and SLP for different horizons and including gear optimization; 40-ton vehicle (left); 80-ton vehicle (right). From top to bottom, the maximum altitude differences are 49 m, 81 m, 93 m and 113 m, respectively, and the maximum velocity limit is 20.83 m/s (75 km/h) for the top figures and 23.61 m/s (85 km/h) for all the other figures. For all cases, the minimum velocity limit is 5 m/s (18 km/h).

B. Implementing the Controller on the High-Fidelity Simulator

The proposed SLP has been tested with a high-fidelity simulation of an 80-ton vehicle with a driving cycle of approximately 150 km. The optimal trajectories of the vehicle velocity and SOC together with the outputs of the third control layer are shown in Fig. 13. The vehicle device actuation is a black box. Here, a high-fidelity complex vehicle model, the Volvo GTT in-house validated simulation model Global Simulation Platform (GSP), has been used to represent the actual vehicle, including the second and third control layers shown in Fig. 5. For the selected driving cycle, a 5% reduction in fuel consumption has been observed as a result of predictive energy management in

addition to a 15% reduction from hybridization and applying the ECMS and instantaneous gear optimization. The reference conventional vehicle follows a varying reference speed profile and the best instantaneous gear selection that together help reduce the fuel consumption by approximately 7% compared to the fuel consumption resulting from following the road speed limit for the 80-ton vehicle. Therefore, the total fuel conservation of the HEV using the predictive energy management compared to a conventional vehicle that tries to follow the road speed limit is 27% for the given powertrain and vehicle, with no reduction in the trip time. The speed-following quality of the second control layer is measured by the RMS of the difference between actual
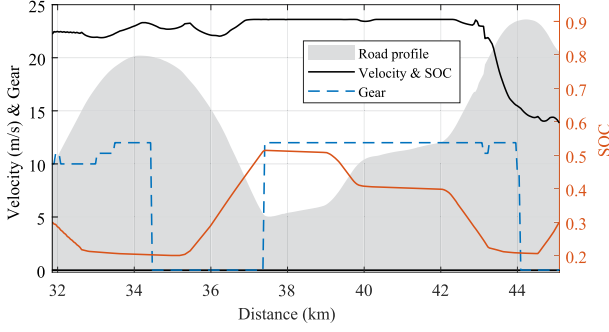
Fig. 9. Example gear trajectory optimized with the SLP. The maximum velocity limit is 23.61 m/s (85 km/h), the minimum velocity limit is 5 m/s (18 km/h), and the maximum elevation difference is 81 m.
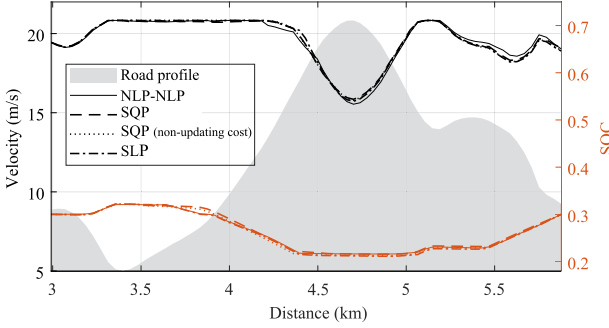

Fig. 10. Best attained and local optimal trajectories compared to the solutions of the SLP and SQP. The maximum velocity limit is 20.83 m/s (75 km/h), the minimum velocity limit is 5 m/s (18 km/h), and the maximum elevation difference is 34 m.
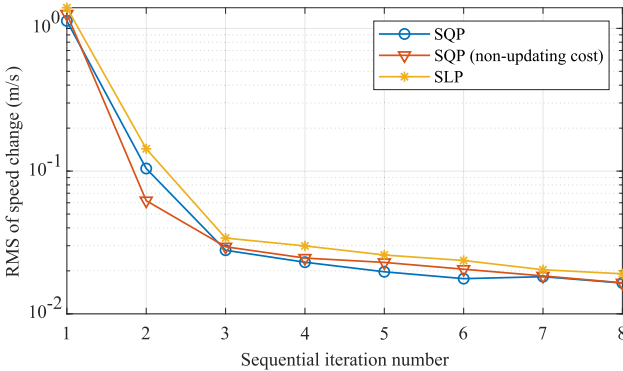

Fig. 11. Sequential convergence of the SQP with an updating cost function, SQP and SLP algorithms including gear optimization. RMS of the speed change is the RMS of the difference between the velocity trajectory found in the current sequential iteration and that found in the next sequential iteration.

and requested speeds, which is approximately 0.6 m/s for the shown driving cycle. If the requested speed is always feasible for the plant vehicle model, then the speed-following quality increases, resulting in an RMS value of approximately 0.1 m/s.

V. DISCUSSION

At each sequential iteration, several computation steps need to be performed. The most expensive step is solving the predictive control problem. Solving the instantaneous gear optimization requires approximately 10% of the time spent on solving the predictive control problem. Another set of computations relates to
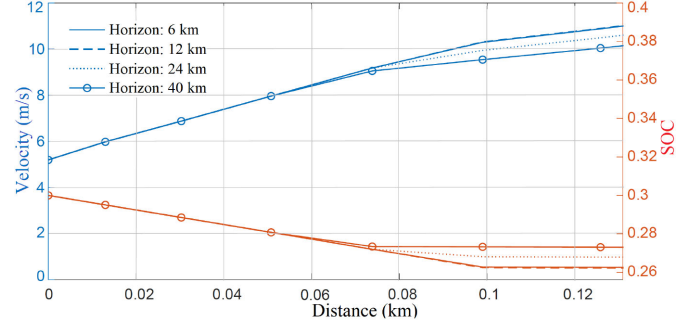

Fig. 12. Optimal velocity and SOC for different horizon lengths. For four road stages, which is equivalent to approximately 75 m here, the optimal trajectories of different horizons are alike. The road topography is shown in Fig. 13 starting from zero position.

the updating of the cost function and constraints. The latter set of computations is heavier in the case of the SQP with an updating cost function due to the additional computations needed for making the problem convex by extracting the positive semidefinite part of the Hessian. Different variants of approximating the Hessian exist in the literature, e.g., the BFGS method, [31]. These types of computations can still be performed in real time onboard the vehicle with a long horizon using the real-time iteration of the SLP/SQP rather than the sequential iterations, as explained by [32]–[34]. The idea of the real-time iteration is to perform one sequential iteration in the current horizon and then let the SQP in the next horizon use the reference values found for the current horizon. In this case, the approximation error will be reduced after several horizons, but the solution may be suboptimal.

Moreover, the SQP with non-updating cost is slightly faster than the SQP with updating cost because it is already convex. In addition, it offers the benefit of not overfitting the noisy measurement data.

The SLP and SQP may give different solutions due to convergence to different local optima. This is because the simplex LP and interior point QP handle initial guesses in different ways. The interior point QP usually does not accept an initial guess as an input. By contrast, a simplex method uses an initial guess. Another reason for the convergence to different local optima is the effect of gear optimization. The gear is optimized in-between SLP/SQP sequential iterations. Since the SLP and SQP converge with different rates, i.e., the SLP generally requires more albeit faster steps, the intermediate gear optimizations may point the solutions in slightly different directions.

Other variables can be used as a state rather than the vehicle velocity, e.g., the vehicle kinetic energy. The advantage of the change of the variable from the velocity to the kinetic energy used by [5], [16] and [17] is the linear relation between the change of the kinetic energy and acceleration, i.e., linear force equilibrium Eq. (1) or linear Eq. (18b). The kinetic energy E_v is given by

$$E_v(s) = \frac{1}{2} m v(s)^2. \tag{45}$$

Using Eq. (14) and noting that $\frac{dv(s)}{ds} = \frac{\dot{v}(t)}{v(t)}$, the derivative of the kinetic energy with respect to the distance traveled is
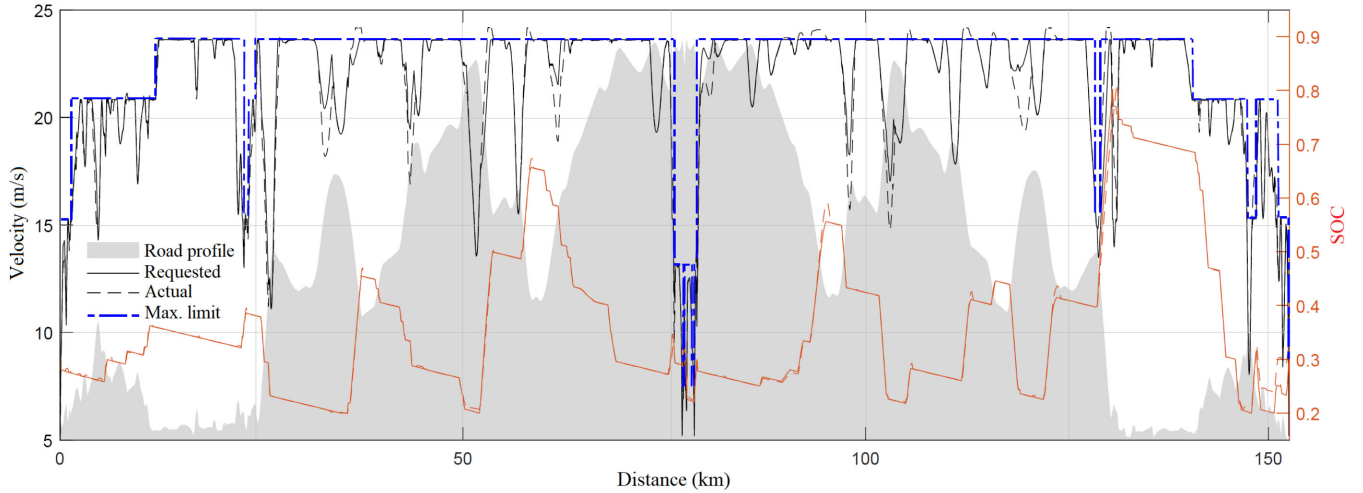
Fig. 13. Requested optimal velocity and SOC trajectories of a 150 km driving cycle together with actual velocity and SOC, i.e., outputs from the third control layer (plant model) shown in Fig. 5.

$$\frac{dE_v(s)}{ds} = mv(s)\frac{dv(s)}{ds} = m\dot{v}(t), \qquad (46)$$

making Eq. (18b) linear.

In [5], using the kinetic energy as a state helped remove the linear interpolation error in DP. By contrast, in the SLP and SQP, there is no need for linear interpolation of states, and the linearization error can be removed by sequential programming. Moreover, in this paper, a good non-updating fit function such as that given by Eq. (43) could not be obtained if the kinetic energy had been used as a state variable rather than the vehicle velocity. Therefore, regardless of the benefit of using the kinetic energy, this paper uses the vehicle velocity as a state. Another type of variable that can be used instead of the vehicle velocity is the inverse of the velocity, which linearizes the time dynamics [35]. However, investigation of the influence of such a change of variables on the convergence rate is outside the scope of this paper and will be pursued in future studies.

Notably, the proposed methodology is not limited exclusively to heavy vehicles and is also valid for light vehicles. However, heavy vehicles benefit more from predictive energy management, including speed profile optimization on hilly roads.

Moreover, it was assumed that the subject vehicle is equipped with driving automation systems of level-2 or higher (i.e., partial or full driving automation according to the SAE standard [36]) that enable following the desired speed, e.g., using a cruise controller. A human driver, if present, can take control of the speed of the vehicle whenever necessary.

The speed limit can be caused either by the legal road speed limit or by the speed of the leading vehicles and is updated in every distance step within the MPC framework. Therefore, the influence of the leading vehicles can be considered via their speed, for example, in a situation in which there is traffic congestion. Additional constraints of keeping the required distance between the vehicles do not need to be included in the first control layer, and in this paper, they were assumed to be handled by the other lower-level vehicle controllers and were hence excluded from the predictive control. However, a constraint on

the time headway can be added in the first control layer since the time is a state as a function of the distance traveled in that layer. The time required for the subject vehicle to reach a certain position must be greater than a given headway plus the time required for the leading vehicle to reach that position, assuming that the time state trajectory of the leading vehicles is known for the controller.

Finally, notably, gear optimization can be performed with DP while preserving the same SLP/SQP algorithm. Moreover, driver comfort penalties (acceleration and jerk) can be included in the cost function of the first control layer without a significant change in computational effort. Additionally, including a penalty on battery energy throughput as a term in the cost function is straightforward, thus taking battery health into consideration according to [14].

VI. CONCLUSION

In this paper, a sequential linear program (SLP) has been proposed for predictive energy management of hybrid electric vehicles. The performance of the method has been assessed by comparison with sequential quadratic programming (SQP). The SLP has been shown to be computationally more efficient by a factor of 4 on average compared to the SQP yet gives trajectories that are very close to the best optimal trajectories attained by the SQP. The generated speed and SOC optimal trajectories, as well as the speed-tracking controller together with the equivalent minimization strategy for following the SOC optimal trajectory, constitute a three-layer control hierarchy that has been tested on a high-fidelity vehicle model, resulting in 5% fuel conservation.

Moreover, two different SQP methods have been introduced with an updating approximating convex function and a fixed approximating function of the fuel rate. Compared to the SLP, the SQP methods need a lower number of sequential iterations to converge, while the SLP is computationally faster.

Future work will extend the application of direct optimal control and the SLP in predictive energy management to include the constraints imposed by lateral dynamics in long heavy vehicles where propelled axles are away from each other with articulation points in between. Moreover, lane change decisions as a result of

traffic situations combined with predictive energy management will be studied by the authors, and the algorithms are planned to be tested on a real-world hybrid heavy vehicle in the future.

APPENDIX A
INITIAL-REFERENCE GENERATION

The initial trajectories of the reference values, i.e., vehicle velocity, ICE gear and engine force, are generated by solving a combination of backward and forward simulation [37] for a conventional reference vehicle. Backward simulation refers to the case when the set acceleration or the set velocity is known and feasible; then, the engine power and torque can be calculated directly if the gear is known. Forward simulation is used when the set acceleration is not feasible. In this case, the actual acceleration is calculated based on the known powertrain limits, e.g., the engine maximum torque and power and the maximum gear ratio. The set velocity v_s can be either the road speed limit or the expected velocity of the driving cycle obtained statistically using the recorded traffic data [38], [39]. In this paper, the combination of backward and forward simulations is summarized according to the following system of equations in the time domain.

$$\dot{v}(t) = \begin{cases} \dot{v}_s(t), & F_{\text{emin}} \le F_{\text{e}}(v(t), t) \le F_{\text{emax}}(v(t)) \\ \frac{F_{\text{ewmax}}(t) - f_{\text{r}}(t)}{m}, & F_{\text{e}}(v(t), t) > F_{\text{emax}}(v(t)) \\ \frac{F_{\text{ewmin}}(t) - f_{\text{r}}(t) + F_{\text{br}}(t)}{m}, & F_{\text{e}}(v(t), t) < F_{\text{emin}} \end{cases}$$
(47a)

$$f_{\text{r}}(t) = mg \sin \alpha(s(t)) + mg f_{\text{r}} \cos \alpha(s(t)) + 0.5 \rho_{\text{a}} A_{\text{f}} c_{\text{d}} v(t)^2$$
(47b)

$$F_{wmax}(t) = \eta_{\text{te}} F_{\text{emax}}(v(t))$$
(47c)

$$F_{wmin}(t) = 0$$
(47d)

$$F_{\text{e}}(v(t), t) = \frac{mv(t) - mv_s(t) + f_{\text{r}}(t)}{\eta_{\text{te}}}$$
(47e)

$$F_{\text{emax}}(v(t)) = \frac{r_{\text{e}}(\gamma_e^*(t))}{R_{\text{w}}} T_{\text{el}}\left(\frac{r_{\text{e}}(\gamma_e^*(t))}{R_{\text{w}}} v(t)\right)$$
(47f)

$$\gamma_e^*(t) = \text{argmax}_{\gamma_e} T_{\text{el}}\left(\frac{r_{\text{e}}(\gamma_e)}{R_{\text{w}}} v(t)\right), \quad \gamma_e \in [1, \dots, 12]$$
(47g)

$$F_{\text{br}}(t) = m\dot{v}_s(t) + f_{\text{r}}(t), \quad F_{\text{br}}(t) \le 0.2 \, mg.$$
(47h)

In Eq. (47h), the maximum brake force is set to 20% of the total possible available brake force to ensure smooth deceleration in case of a sudden change in the set speed. System of equations (47) must be integrated forward in time form the start to the end of the driving cycle s_{f}, i.e., from t_0 to t_{f}, where $s_{\text{f}} = \int_{t_0}^{t_f} v(t) dt$ and $v(t_0) = v_s(t_0)$. Furthermore, the reference trajectory of the engine equivalent force $\hat{F}_{\text{e}}(t)$ can be calculated:

$$\hat{F}_{\text{e}}(t) = \frac{m\dot{v}(t) + f_{\text{r}}(t)}{\eta_{\text{te}}}.$$
(48)

Conversion from the time to space domain can be done using Eq. (14). Knowing the reference velocity and engine equivalent force, optimization problem (19) can be solved to obtain the initial reference gear trajectory $\hat{\gamma}_{\text{e}}(s)$. Finally, the initial brake

force, equivalent EM force and SOC reference trajectory are set to $\hat{F}_{\text{br}}(s) = 0$, $\hat{F}_{\text{m}}(s) = 0$ and $s\hat{o}c(s) = soc_0$.

Notably, solving Eq. (47) is only necessary for the calculation of $t_{\text{tref}} = t_{\text{f}}$ and setting constraint Eq. (18i). Generally, initial reference trajectories do not need to be calculated and can be set arbitrarily. For example, the reference speed can be set to the road legal limit, $\hat{F}_{\text{e}}(t) = 0$ and $\hat{\gamma}_{\text{e}}(s) = 10$ can be taken. The gear $\hat{\gamma}_{\text{e}}(s)$ should be feasible for the entire driving cycle.

APPENDIX B
DERIVING THE EM-CONSUMED POWER MAP BASED ON THE EM EFFICIENCY MAP

If the measurement data of the power losses in the EM are provided based on the efficiency η_{m} rather than on the consumed power, then the conversion can be performed according to the following.

$$P_{\text{mc}}(\omega_{\text{m}}, T_{\text{m}}) = \begin{cases} \frac{\omega_{\text{m}} T_{\text{m}}}{\eta_{\text{m}}(\omega_{\text{m}}, T_{\text{m}})}, & T_{\text{m}} > 0 \\ \omega_{\text{m}} T_{\text{m}} \eta_{\text{m}}(\omega_{\text{m}}, T_{\text{m}}), & T_{\text{m}} \le 0. \end{cases}$$
(49)

However, a problem occurs when the torque is zero, where efficiency is not defined while losses can be nonzero. Then, the consumed power at zero torque can be calculated by data interpolation similar to Eq. (7).

ACKNOWLEDGEMENT

REFERENCES

[1] European Commission, "Road transport: Reducing CO$_2$ emissions from vehicles," 2016. [Online]. Available: https://ec.europa.eu/clima/policies/transport/vehicles_en

[2] A. Schwarzkopf and R. Leipnik, "Control of highway vehicles for minimum fuel consumption over varying terrain," *Transp. Res.*, vol. 11, no. 4, pp. 279–286, 1977.

[3] V. Monastyrsky and I. Golownykh, "Rapid computation of optimal control for vehicles," *Transp. Res. Part B: Methodological*, vol. 27, no. 3, pp. 219–227, 1993.

[4] A. Fröberg, E. Hellström, and L. Nielsen, "Explicit fuel optimal speed profiles for heavy trucks on a set of topographic road profiles," SAE World Congress, no. 2006-01-1071, 2006.

[5] E. Hellström, J. Åslund, and L. Nielsen, "Design of an efficient algorithm for fuel-optimal look-ahead control," *Control Eng. Pract.*, vol. 18, no. 11, pp. 1318–1327, 2010.

[6] L. Serrao, S. Onori, and G. Rizzoni, "A comparative analysis of energy management strategies for hybrid electric vehicles," *J. Dyn. Syst., Meas., Control*, vol. 133, no. 3, 2011, pp. 0310121–0310129.

[7] M. Diehl, H. J. Ferreau, and N. Haverbeke, "Efficient numerical methods for nonlinear MPC and moving horizon estimation," in *Proc. Nonlinear Model Predictive Control*, 2009, pp. 391–417.

[8] M. Diehl, H. G. Bock, H. Diedam, and P.-B. Wieber, "Fast direct multiple shooting algorithms for optimal robot control," in *Fast Motions Biomech. Robot.*, 2006, pp. 65–93.

[9] J. Ritzmann, A. Christon, M. Salazar, and C. Onder, "Fuel-optimal power split and gear selection strategies for a hybrid electric vehicle," SAE Technical Paper 2019-24-0205, 2019, pp. 1–11.

[10] V. van Reeven and T. Hofman, "Multi-level energy management for hybrid electric vehicles—Part I," Vehicles, vol. 1, no. 1, pp. 3–40, 2019.

[11] T. van Keulen, J. Gillot, B. de Jager, and M. Steinbuch, "Solution for state constrained optimal control problems applied to power split control for hybrid vehicles," *Automatica*, vol. 50, no. 1, pp. 187–192, 2014.

[12] C.-C. Lin, J.-M. Kang, J. W. Grizzle, and H. Peng, "Energy management strategy for a parallel hybrid electric truck," in *Proc. IEEE Amer. Control Conf.*, vol. 4, pp. 2878–2883, 2001.

[13] O. Sundström, "Optimal control and design of hybrid-electric vehicles," PhD dissertation, ETH Zurich, Dept. Inst. Dynamic Syst. Cont., 2009.

[14] T. Ghandriz, L. Laine, J. Hellgren, and B. Jacobson, "Sensitivity analysis of optimal energy management in plug-in hybrid heavy vehicles," in *Proc. 2nd IEEE Int. Conf. Intell. Transp. Eng.*, 2017, pp. 320–327.

[15] L. Johannesson, M. Asbogard, and B. Egardt, "Assessing the potential of predictive control for hybrid vehicle powertrains using stochastic dynamic programming," *IEEE Trans. Intell. Transp. Syst.*, vol. 8, no. 1, pp. 71–83, 2007.

[16] L. Johannesson, N. Murgovski, E. Jonasson, J. Hellgren, and B. Egardt, "Predictive energy management of hybrid long-haul trucks," *Control Eng. Pract.*, vol. 41, pp. 83–97, 2015.

[17] N. Murgovski, B. Egardt, and M. Nilsson, "Cooperative energy management of automated vehicles," *Control Eng. Pract.*, vol. 57, pp. 84–98, 2016.

[18] S. Uebel, N. Murgovski, C. Tempelhahn, and B. Bäker, "Optimal energy management and velocity control of hybrid electric vehicles," *IEEE Trans. Veh. Technol.*, vol. 67, no. 1, pp. 327–337, Jan. 2018.

[19] A. A. Malikopoulos, "Supervisory power management control algorithms for hybrid electric vehicles: A survey," *IEEE Trans. Intell. Trans. Syst.*, vol. 15, no. 5, pp. 1869–1885, Oct. 2014.

[20] B. De Jager, T. Van Keulen, and J. Kessels, *Optimal Control of Hybrid Vehicles*. Berlin, Germany: Springer, 2013.

[21] M. Pourabdollah, B. Egardt, N. Murgovski, and A. Grauers, "Convex optimization methods for powertrain sizing of electrified vehicles by using different levels of modeling details," *IEEE Trans. Veh. Technol.*, vol. 67, no. 3, pp. 1881–1893, Mar. 2018.

[22] E. Hellström, J. Åslund, and L. Nielsen, "Management of kinetic and electric energy in heavy trucks," *SAE Int. J. Engines*, vol. 3, no. 1, pp. 1152–1163, 2010.

[23] M. Hovgard, O. Jonsson, N. Murgovski, M. Sanfridson, and J. Fredriksson, "Cooperative energy management of electrified vehicles on hilly roads," *Control Eng. Pract.*, vol. 73, pp. 66–78, 2018.

[24] B. Jacobson and M. Spickenreuther, "Gearshift sequence optimisation for vehicles with automated non-powershifting transmissions," *Int. J. Veh. Des.*, vol. 32, no. 3-4, pp. 187–207, 2003.

[25] M. Zhu, H. Chen, and G. Xiong, "A model predictive speed tracking control approach for autonomous ground vehicles," *Mech. Syst. Signal Process.*, vol. 87, pp. 138–152, 2017.

[26] G. Paganelli, G. Ercole, A. Brahma, Y. Guezennec, and G. Rizzoni, "General supervisory control policy for the energy optimization of charge-sustaining hybrid electric vehicles," *JSAE Rev.*, vol. 22, no. 4, pp. 511–518, 2001.

[27] G. Paganelli, T. M. Guerra, S. Delprat, J.-J. Santin, M. Delhom, and E. Combes, "Simulation and assessment of power control strategies for a parallel hybrid car," *Proc. Inst. Mech. Engineers, Part D: J. Automobile Eng.*, vol. 214, no. 7, pp. 705–717, 2000.

[28] J. Nocedal and S. Wright, *Numerical Optimization*. New York, NY, USA: Springer Science & Business Media, 2006.

[29] B. Egardt, N. Murgovski, M. Pourabdollah, and L. J. Mardh, "Electromobility studies based on convex optimization: Design and control issues regarding vehicle electrification," *IEEE Control Syst. Mag.*, vol. 34, no. 2, pp. 32–49, Apr. 2014.

[30] N. Murgovski, L. Johannesson, X. Hu, B. Egardt, and J. Sjöberg, "Convex relaxations in the optimal control of electrified vehicles," in *Proc. Amer. Control Conf.*, 2015, pp. 2292–2298.

[31] R. Fletcher, *Practical Methods of Optimization*. Hoboken, NJ, USA: Wiley, 2013.

[32] M. Diehl, "Real-time optimization for large scale nonlinear processes," PhD dissertation, Dept. Applied Math., The Faculty of Mathematics and Computer Science, Heidelberg University, 2001.

[33] M. Diehl, R. Findeisen, F. Allgöwer, H. G. Bock, and J. P. Schlöder, "Nominal stability of real-time iteration scheme for nonlinear model predictive control," *IEE Proc.-Control Theory Appl.*, vol. 152, no. 3, pp. 296–308, 2005.

[34] S. Gros, M. Zanon, R. Quirynen, A. Bemporad, and M. Diehl, "From linear to nonlinear mpc: Bridging the gap via the real-time iteration," *Int. J. Control*, vol. 93, no. 1, pp. 62–80, 2020.

[35] J. Karlsson, N. Murgovski, and J. Sjöberg, "Computationally efficient autonomous overtaking on highways," *IEEE Trans. Intell. Transp. Syst.*, vol. 21, no. 8, pp. 3169–3183, Aug. 2020.

[36] *SAE standard*, "Taxonomy and definitions for terms related to on-road motor vehicle automated driving systems," SAE Standard J, vol. 3016, pp. 1–16, 2016.

[37] K. B. Wipke, M. R. Cuddy, and S. D. Burch, "Advisor 2.1: A user-friendly advanced powertrain simulation using a combined backward/forward approach," *IEEE Trans. Veh. Technol.*, vol. 48, no. 6, pp. 1751–1761, Nov. 1999.

[38] V. Larsson, L. J. Mårdh, B. Egardt, and S. Karlsson, "Commuter route optimized energy management of hybrid electric vehicles," *IEEE Trans. Intell. Trans. Syst.*, vol. 15, no. 3, pp. 1145–1154, 2014.

[39] P. Pettersson, P. Johannesson, B. Jacobson, F. Bruzelius, L. Fast, and S. Berglund, "A statistical operating cycle description for prediction of road vehicles' energy consumption," *Transp. Res. Part D: Transp. Environ.*, vol. 73, pp. 205–229, 2019.

Toheed Ghandriz received the M.Sc. degree in mechanical engineering from the Blekinge Institute of Technology, Karlskrona, Sweden, in 2014. He is currently working toward the Ph.D. degree in vehicle dynamic with the Chalmers University of Technology, Gothenburg, Sweden. From 2014 to 2015, he was a R&D Mechanical Development Engineer with Dassault Systémes, Lund, Sweden. His research interests include optimal distribution of propulsion over axles in long combination vehicles considering energy, dynamic performance, and transport economy.

Bengt Jacobson received the Ph.D. degree in machine elements from the Chalmers University of Technology, Gothenburg, Sweden, in 1993. From 2001 to 2010, he was a Technical Expert with Volvo Car Corporation, Gothenburg, Sweden, with a focus on vehicle dynamics control and active safety. He is currently a Professor of vehicle dynamics with the Department of Mechanics and Maritime Sciences, Chalmers University of Technology.

Nikolce Murgovski received the M.Sc. degree in software engineering from University West, Trollähttan, Sweden, in 2007, and the M.Sc. degree in applied physics and the Ph.D. degree in signals and systems from the Chalmers University of Technology, Gothenburg, Sweden, in 2007 and 2012, respectively. He is currently an Assistant Professor with the Department of Signals and Systems, Chalmers University of Technology. His research focuses on optimization and optimal control in the automotive area.

Leo Laine received the Ph.D. degree in hybrid electric vehicles, illustrating how vehicle stability control is balanced with energy management for over-actuated vehicles from the Chalmers University of Technology, Gothenburg, Sweden. Since 2007, he has been with Volvo Group Trucks Technology in Chassis as a Senior Technology Specialist within complete powertrain and vehicle control. Since 2013, he has also been an Adjunct Professor of vehicle dynamics with Chalmers Vehicle Engineering and Autonomous Systems.

Peter Nilsson received the Ph.D. degree in machine and vehicle systems from the Chalmers University of Technology, Gothenburg, Sweden, in 2017. Since 2002, he has been with Volvo Group Trucks Technology, Gothenburg, Sweden. From 2002 to 2012, he was a Senior Vehicle Analyst of vehicle dynamics and noise and vibration isolation. Since 2017, he has been working on vehicle planning and control within autonomous solutions.